# Ozone variability in the troposphere and the stratosphere from the first six years of IASI observations (2008-2013)

C. Wespes[1], D. Hurtmans[1], L.K. Emmons[2], S. Safieddine[3*], C. Clerbaux[1,3], D. P. Edwards[2] and P.-F. Coheur[1]

[1]Spectroscopie de l'Atmosphère, Service de Chimie Quantique et Photophysique, Université Libre de Bruxelles (U.L.B.), Brussels, Belgium

[2]National Center for Atmospheric Research, Boulder, CO, USA

[3]Sorbonne Universités, UPMC Univ. Paris 06; Université Versailles St-Quentin; CNRS/INSU, LATMOS-IPSL, Paris, France

*Now at Department of Civil and Environmental Engineering, Institute of Technology, Cambridge, Massachusetts, United States

## Abstract

In this paper, we assess how daily ozone ($O_3$) measurements from the Infrared Atmospheric Sounding Interferometer (IASI) on the MetOp-A platform can contribute to the analyses of the processes driving $O_3$ variability in the troposphere and the stratosphere and, in the future, to the monitoring of long-term trends. The temporal evolution of $O_3$ during the first 6 years of IASI (2008-2013) operation is investigated with multivariate regressions separately in four different layers (ground-300 hPa, 300-150 hPa, 150-25 hPa, 25-3 hPa), by adjusting to the daily time series averaged in 20° zonal bands, seasonal and linear trend terms along with important geophysical drivers of $O_3$ variation (e.g. solar flux, quasi biennial oscillations). The regression model is shown to perform generally very well with a strong dominance of the annual harmonic terms and significant contributions from $O_3$ drivers, in particular in the equatorial region where the QBO and the solar flux contribution dominate. More particularly, despite the short period of IASI dataset available to now, two noticeable statistically significant apparent trends are inferred from the daily IASI measurements: a positive trend in the upper stratosphere (e.g. 1.74±0.77 DU/yr between 30°S-50°S) which is consistent with other studies suggesting a turnaround for stratospheric $O_3$ recovery, and a negative trend in the troposphere at the mid-and high northern

latitudes (e.g. -0.26±0.11 DU/yr between 30°N-50°N), especially during summer and probably linked to the impact of decreasing ozone precursor emissions. The impact of the high temporal sampling of IASI on the uncertainty in the determination of $O_3$ trend has been further explored by performing multivariate regressions on IASI monthly averages and on ground-based FTIR measurements.

## 1 Introduction

Global climate change is one of the most important environmental problems of today and monitoring the behavior of the atmospheric constituents (radiatively active gases and those involved in their chemical production) is key to understand the present climate and apprehend future climate changes. Long-term measurements of these gases are necessary to study the evolution of their abundance, changing sources and sinks in the atmosphere.

As a reactive trace gas present simultaneously in the troposphere and in the stratosphere, $O_3$ plays a significant role in atmospheric radiative forcing, atmospheric chemistry and air quality. In the stratosphere, $O_3$ is sensitive to changes in (photo-)chemical and dynamical processes and, as a result, undergoes large variations on seasonal and annual time scales. Measurements of $O_3$ total column have indicated a downward trend in stratospheric ozone over the period from 1980s to the late 1990s relative to the pre-1980 values, which is due to the growth of the reactive bromine and chlorine species following anthropogenic emissions during that period (WMO, 2003). In response to the 1987 Montreal Protocol and its amendments, with a reduction of the Ozone-Depleting Substances (ODS; Newchurch et al., 2003), a recovery of stratospheric ozone concentrations to the pre-1980 values is expected (Hofmann, 1996). While earlier works have debated a probable turnaround for the ozone hole recovery (e.g. Hadjinicolaou et al., 2005; Reinsel et al., 2002; Stolarski and Frith, 2006), WMO already indicated in 2007 that the total ozone in the 2002-2005 period was no longer decreasing, reflecting such a turnaround. Since then several studies have shown successful identification of ozone recovery over Antarctica and over northern latitudes (e.g. Mäder et al., 2010; Salby et al., 2011; WMO, 2011; Kuttippurath et al., 2013; Knibbe et al., 2014; Shepherd et al., 2014). Nevertheless, the most recent papers as well as the WMO 2014 ozone assessment have warned, because of possible underestimation of

the true uncertainties in the ozone trends attributed to decreasing Effective Equivalent Stratospheric Chlorine (EESC), against overly optimistic conclusions with regard to a possible increase in Antarctic stratospheric ozone (Kramarova et al., 2014 ; WMO, 2014; Knibbe et al., 2014; de Laat et al., 2015; Kuttippurath et al., 2015; Varai et al., 2015). The causes of the observed stratospheric $O_3$ changes are hard to isolate and remain uncertain precisely considering the contribution of dynamical variability to the apparent trend and the limitations of current chemistry-climate models to reproduce the observations. The assessment of ozone trends in the troposphere is even more challenging due to the influence of many simultaneous processes (e.g. emission of precursors, long-range transport, stratosphere-troposphere exchanges –STE–), which are all strongly variable temporally and spatially (e.g. Logan et al., 2012; Hess and Zbinden, 2013; Neu et al., 2014). Overall, there are still today large differences in the value of the $O_3$ trends determined from independent studies and datasets (mostly from ground-based and satellite observations) in both the stratosphere and the troposphere (e.g. Oltmans et al., 1998; 2006; Randel and Wu, 2007; Gardiner et al., 2008; Vigouroux et al., 2008; Jiang et al., 2008; Kyrölä et al., 2010; Vigouroux et al., 2014). In order to improve on this and because $O_3$ has been recognized as a Global Climate Observing System (GCOS) Essential Climate Variables (ECVs), the scientific community has underlined the need of acquiring high quality global, long-term and homogenized ozone profile records from satellites (Randel and Wu, 2007; Jones et al., 2009; WMO, 2007; 2011; 2014). This specifically has resulted in the ESA Ozone Climate Change Initiative ($O_3$-CCI; http://www.esa-ozone-cci.org/).

The Infrared Atmospheric Sounding Interferometer (IASI) onboard the polar orbiting MetOp, with its unprecedented spatiotemporal sampling of the globe, its high radiometric stability and the long duration of its program (3 successive instruments to cover 15 years) provides in principle an excellent means to contribute to the analyses of the $O_3$ variability and trends. This is further strengthened by the possibility of using IASI measurements to discriminate $O_3$ distributions and variability in the troposphere and the stratosphere, as shown in earlier studies (Boynard et al., 2009; Wespes et al., 2009; Dufour et al, 2010 ; Barret et al., 2011; Scannell et al., 2012; Wespes et al., 2012; Safieddine et al., 2013). Here, we use the first 6 years (2008-2013) of the new $O_3$ dataset provided by IASI on MetOp-A to perform a first analysis of the $O_3$

time development in the stratosphere and in the troposphere. This is achieved globally by using zonal averages in 20° latitude bands and a multivariate linear regression model which accounts for various natural cycles affecting $O_3$. We also explore in this paper to which extent the exceptional temporal sampling of IASI can counterbalance the short period of data available for assessing trends in partial columns.

In section 2, we give a short description of IASI and of the $O_3$ retrieved columns used here. Section 3 details the multivariate regression model used for fitting the time series. In Section 4, we evaluate how the ozone natural variability is captured by IASI and we present the time evolution of the retrieved $O_3$ profiles and of four partial columns (Upper Stratosphere –UST-; Middle-Low Stratosphere –MLST–; Upper Troposphere Lower Stratosphere –UTLS–; Middle-Low Troposphere –MLT–) using 20-degree latitudinal averages on a daily basis. The apparent dynamical and chemical processes in each latitude band and vertical layer are then analyzed on the basis of the multiple regression results using a series of common geophysical variables. The "standard" contributors in the fitted time series, as well as a linear trend term, are analyzed in the specified altitude layers. Finally, the trends inferred from IASI are compared against those from FTIR for six stations in the northern hemisphere.

## 2 IASI measurements and retrieval method

IASI measures the thermal infrared emission of the Earth-atmosphere between 645 and 2760 $cm^{-1}$ with a field of view of 2×2 circular pixels on the ground, each of 12 km diameter at nadir. The IASI measurements are taken every 50 km along the track of the satellite at nadir, but also across-track over a swath width of 2200 km. IASI provides a global coverage twice a day with overpass times at 9:30 and 21:30 mean local solar time. The instrument is also characterized by a high spectral resolution which allows the retrieval of numerous gas-phase species (e.g. Clerbaux et al., 2009; Clarisse et al., 2012).

Ozone profiles are retrieved with the Fast Optimal Retrievals on Layers for IASI (FORLI) software developed at ULB/LATMOS. FORLI relies on a fast radiative transfer and on a retrieval methodology based on the Optimal Estimation Method (Rodgers, 2000). In the version

used in this study (FORLI-$O_3$ v20100815), the $O_3$ profile is retrieved for individual IASI measurement on a uniform 1 km vertical grid on 40 layers from surface up to 40 km. The a priori information (a priori profile and a priori covariance matrix) is built from the Logan/Labow/McPeters climatology (McPeters et al., 2007) and only one single $O_3$ a priori profile and variance-covariance matrix are used. The retrieval parameters and performances are detailed in Hurtmans et al. (2012). The FORLI-$O_3$ profiles and/or total and partial columns have undergone validation using available ground-based, aircraft, $O_3$ sonde and other satellite observations (Anton et al., 2011; Dufour et al., 2012; Gazeaux et al., 2012; Parrington et al., 2012; Pommier et al., 2012; Scannell et al., 2012; Oetjen et al., 2014). Generally, the results show good agreements between FORLI-$O_3$ and independent measurements with a low bias (<10%) in the total column and in the vertical profile, except in UTLS where a positive bias of 10-15% is reported (Dufour et al., 2012; Gazeaux et al., 2012; Oetjen et al., 2014).

In this study, only daytime $O_3$ IASI observations from good spectral fits (RMS of the spectral residual lower than $3.5\times10^{-8}$ W/cm$^2$.sr.cm$^{-1}$) have been analyzed. Daytime IASI observations (determined with a solar zenith angle to the sun < 80°) are characterized by a better vertical sensitivity to the troposphere associated with a higher surface temperature and a higher thermal contrast (Clerbaux et al., 2009; Boynard et al., 2009). Furthermore, cloud contaminated scenes with cloud cover < 13% (Hurtmans et al., 2012) were removed using cloud information from the Eumetcast operational processing (August et al., 2012).

An example of typical FORLI-$O_3$ averaging kernel functions for one mid-latitude observation in July (45°N/66°E) is represented on Fig.1. The layers have been defined as: ground-300hPa (MLT), 300-150hPa (UTLS), 150-25 hPa (MLST) and above 25 hPa (UST), so that they are characterized by a DOFS (Degrees Of Freedom for Signal) close to 1 with a maximum sensitivity approximatively in the middle of the layers, except for the 300-150 hPa layer which has a reduced sensitivity. Taken globally, the DOFS for the entire profile ranges from ~2.5 in cold polar regions to ~4.5 in hot tropical regions, depending mostly on surface temperature, with a maximum sensitivity in the upper troposphere and in the lower stratosphere (Hurtmans et al., 2012). In the MLT, the maximum of sensitivity is around 4–8 km altitude for almost all

situations (Wespes et al., 2012). The sharp decrease of sensitivity down to the surface is inherent to nadir thermal IR sounding in cases of low surface temperature or low thermal contrast and indicates that the retrieved information principally comes from the a priori in the lowest layer. Figure 2 presents July 2010 global maps of averaged FORLI-$O_3$ partial columns for two partial layers (MLT and MLST), and of the associated DOFS and *a priori* contribution (calculated as $X_a$-**A**($X_a$), where $X_a$ is the *a priori* profile and **A**, the averaging kernel matrix, following the formalism of Rodgers (2000)). The two layers exhibit different sensitivity patterns: in the MLT, the DOFS typically range from 0.4 in the cold polar regions to 1 in regions characterized by high thermal contrast with medium humidity, such as the mid-latitude continental Northern Hemisphere (N.H.) (Clerbaux et al., 2009). Lower DOFS values in the intertropical belt are explained by overlapping water vapor lines. In contrast, the DOFS for the MLST are globally almost constant and close to one, with only slightly lower values (0.9) over polar regions. The *a priori* contribution is anti-correlated with the sensitivity, as expected. It ranges between a few % to ~30% and does not exceed 20% on 20° zonal averages in the troposphere (see Supporting Information; Fig. S3, dashed lines), while the a priori contribution is smaller than ~12% in the middle stratosphere. These findings indicate that the IASI MLST time series should accurately represent stratospheric variations, while the time series in the troposphere may reflect to some extent variations from the upper layers in addition to the real variability in the troposphere. In order to quantify this effect, the contribution of the stratosphere into the tropospheric ozone as seen by IASI has been estimated with a global 3-D chemical transport model (MOZART-4). Details of the model-observation comparisons can be found in the Supplement (see Fig. S2 and S3). We interestingly show that the stratospheric contribution to the MLT columns measured by IASI varies between 30% and 60%, depending on latitude and season (Fig. S5). The limited vertical sensitivity of IASI contributes to this by a smaller part (~10%-20%) than the natural stratospheric influence (~20% to 45%) (See Fig. S4 and S5). In addition, we find that the contribution of the natural variability (from both the troposphere and the stratosphere) on the MLT $O_3$ columns is larger than 50% everywhere. In the 30N-50N band where the DOFS is the largest (See Fig.2 (b)), this contribution reaches ~85% from which ~20-35% originates from the stratosphere and ~55% from the troposphere (Fig.S6 (a) and (b)). Nevertheless, the

contamination of IASI MLT $O_3$ with variations in stratospheric $O_3$ has to be kept in mind when analyzing IASI MLT $O_3$.

## 3 Fitting method

### 3.1. Statistical model

In order to characterize the changes in ozone measured by IASI and to allow a proper separation of trend, we use a multiple linear regression model accounting for a linear trend and for inter-annual, seasonal and non-seasonal variations related to physical processes that are known to affect the ozone records. More specifically, the time series analysis is based on the fitting of daily (or monthly) median partial columns in different latitude bands following:

$$O_3(t) = Cst + x_1 \cdot trend + \sum_{n=1,2}\left[a_n \cdot \cos(n\omega t) + b_n \cdot \sin(n\omega t)\right] + \sum_{j=2}^{m} x_j X_{norm,j}(t) + \varepsilon(t) \quad (1)$$

where $t$ is the number of days (or months), $x_1$ is the 6-year trend coefficient in the data, $\omega$ = $2\pi/365.25$ for the daily model (or $2\pi/12$ for the monthly model) and $X_{norm,j}$ are independent geophysical variables, the so-called "explanatory variables" or "proxies", which are in this study normalized over the period of IASI observation (2008-2013), as:

$$X_{norm}(t) = 2\left[X(t) - X_{median}\right] / \left[X_{\max} - X_{\min}\right] \quad (2)$$

$\varepsilon(t)$ in Eq. (1) represents the residual variation which is not described by the model and which is assumed to be autoregressive with time lag of 1 day (or 1 month). The constant term ($Cst$) and the coefficients $a_n, b_n, x_j$ are estimated by least-squares method and their standard errors ($\sigma_e$) are calculated from the covariance matrix of the coefficients and corrected to take into account the uncertainty due to the autocorrelation of the noise residual as discussed in Santer et al. (2000) and references therein:

$$\sigma_e^2 = (Y^T Y)^{-1} \cdot \frac{\sum_t \left[O_3(t) - yY(t)\right]^2}{n-m} \cdot \frac{1+\Phi}{1-\Phi} \quad (3)$$

Where $Y$ is the matrix with the covariates $(trend, \cos(n\omega t), \sin(n\omega t), X_{norm,j})$ sorted by column, $y$ is the vector of the regression coefficients corresponding to the columns of $Y$, n is the

number of daily (or monthly) data points in the time series, m is the number of the fitted parameters, and $\Phi$ is the lag-1 autocorrelation of the residuals.

The median is used as a statistical average since it is more robust against the outliers than the normal mean (Kyrölä et al., 2006; 2010). Note that, similarly to Kyrölä et al. (2010), the model has been applied on $O_3$ mixing ratios rather than on partial columns but without significant improvement on the fitting residuals and R values.

### 3.2. Geophysical variables

In Eq. (1), harmonic time series with a period of a year and a half year are used to account for the Brewer-Dobson circulation and the solar insolation ($a_1$ and $b_1$ coefficients), and for the meridional circulation ($a_2$ and $b_2$ coefficients), respectively (Kyrölä et al., 2010). While these effects are of a periodic nature, the geophysical variables ( $X_j$ ) are used here to parameterize the ozone variations on non-seasonal timescales. The chosen proxies are $F_{10.7}, QBO^{10}, QBO^{30}, ENSO$, *NAO/AAO*, the first three being the most commonly used ("standard") proxies to describe the natural ozone variability, i.e. the solar radio flux at 10.7 cm and the quasi-biennial oscillation (*QBO*) which is represented by two orthogonal zonal components of the equatorial stratospheric wind measured at 10 hPa and 30 hPa, respectively (e.g. Randel and Wu, 2007). The three other proxies, *ENSO, NAO* and *AAO*, are used to account for other important fluctuating dynamical features: the El Niño/Southern Oscillation, the North Atlantic Oscillation and the Antarctic Oscillation, respectively. Table 1 lists the selected proxies, their sources and their resolutions. The time series of these proxies normalized over the 2000-2013 period following Eq. 2 are shown in Fig.3 (a) and (b) and they are shortly described hereafter:

- *Solar flux*: the F10.7 cm solar radio flux is an excellent indicator of solar activity and is commonly used to represent the 11 year solar cycle. It is available from continuous consistent routine measurements at the Penticton Radio Observatory in British Columbia which are corrected for the variable Sun-Earth distance resulting from the eccentric orbit of the Earth around the Sun. Over the period 2008-2013, the radio solar flux increases from about 65 units in 2008 to 180 units in 2013 and is characterized by a specific daily "fingerprint" (see Fig.3 (a)). Note that because the period of IASI observations does not cover a full 11 year solar cycle, it

could affect the determination of the trend in the regression procedure. The difficulty in discriminating the solar flux and linear trend terms is a known problem for such multivariate regression: it feeds into their uncertainties and it can lead to biases in the coefficients determination (e.g. Soukharev et al., 2006).

- *QBO terms*: The QBO of the equatorial winds is a main component of the dynamics of the tropical stratosphere (Chipperfield et al., 1994; 2003; Randel and Wu, 1996; 2007; Logan et al., 2003; Tian et al., 2006; Fadnavis and Beig, 2009; Hauchecorne et al., 2010). It strongly influences the distributions of stratospheric $O_3$ propagating alternatively westerly and easterly with a mean period of 28 to 29 months. Positive and negative vertical gradients alternate periodically. At the top of the vertical QBO domain, there is a predominance of easterlies, while, at the bottom, westerly winds are more frequent. In order to account for the out-of-phase relationship between the QBO periodic oscillations in the upper and in the lower stratosphere, orthogonal zonal winds measured at 10hPa (Fig.3a; orange) and 30hPa (Fig.3a; green) by the ground-station in Singapore have been considered here (Randel and Wu, 1996; Hood and Soukharev, 2006).

- *NAO, AAO and ENSO*: The El Niño/Southern Oscillation is represented by the 3-month running mean of Sea Surface Temperature (SST) anomalies (in degrees Celsius) in the Niño region 3.4 (region bounded by 120°W-170°W and 5°S- 5°N). Raw data are taken from marine ships and buoys observations. The North Atlantic and Antarctic Oscillations are described by the daily (or monthly) NAO and AAO indices which are constructed from the daily (or monthly) mean 500 hPa geopotential height anomalies in the 20°N-90°N region and 700 hPa height anomalies in the S.H. (Southern Hemisphere), respectively. Detailed information for these proxies can be found in http://www.cpc.ncep.noaa.gov/. These proxies describe important dynamical features which affect ozone distributions in both the troposphere and the lower stratosphere (e.g. Weiss et al., 2001, Frossard et al., 2013; Rieder et al., 2013; and references therein). The daily or 3-monthly average indexes used to parameterize these fluctuations are shown in Fig. 3 (b). The NAO and AAO indexes are used for the N.H. and the S.H., respectively (both are used for the equatorial band). These proxies have been included in the statistical model for completeness even if they are expected to only have a weak apparent contribution to the IASI ozone time series due to their large spatial variability in a zonal band (e.g. Frossard et al., 2013;

Rieder et al., 2013). We have verified that including a typical time-lag relation between ozone and the ENSO variable from 0 to 4 months did not improve the regression model in terms of residuals and uncertainty of the fitted parameters. As a consequence, a time-lag has not been taken into account in our study.

- *Effective equivalent stratospheric chlorine (EESC)*: The EESC is a common proxy used for describing the influence of the ODS in $O_3$ variations. However, because the IASI time series starts several years after the turnaround for the ozone hole recovery in 1996/1997 (WMO, 2010), their influence is not represented by a dedicated proxy but is rather accounted for by the linear trend term.

Even if some of the above proxies are only specific to processes occurring in the stratosphere, we adopt the same approach (geophysical variables, model and regression procedure) for adjusting the IASI $O_3$ time series in the troposphere. This proves useful in particular to account for the stratospheric contribution to the tropospheric layer (~30-60%; see Section 2 and Supporting Information, Fig. S5) due to stratosphere-troposphere exchanges (STE) and to the fact that this tropospheric layer is not perfectly decorrelated from the stratosphere. This has to be kept in mind when analyzing the time series in the troposphere in Section 4. Specific processes in the troposphere such as emissions of ozone precursors, long-range transport and in situ chemical processing are taken into account in the model in the harmonic and the linear trend terms of the Eq. 1 (e.g. Logan et al., 2012). Including harmonic terms having 4- and 3-month periods in the model has been tested to describe $O_3$ dependency on shorter scales (e.g. Gebhardt et al., 2014), but this did not improved the results in terms of residuals and uncertainty of correlation coefficients.

### 3.3. Iterative backward variable selection

Similarly to previous studies (e.g. Steinbrecht et al., 2004; Mäder et al. 2007, 2010; Knibbe et al., 2014), we perform an iterative stepwise backward elimination approach, based on p-values of the regression coefficients for the rejection, to select the most relevant combination of the above described regression variables (harmonic, linear and explanatory) to fit the observations. The minimum p-value for a regression term to be removed (exit tolerance) is set at 0.05, which

corresponds to a significance of 95%. The initial model which includes all regression variables is fitted first. Then, at each iteration, the variables characterized by p-values larger than 5% are rejected. At the end of the iterative process, the remaining terms are considered to have significant influence on the measured $O_3$ variability while the rejected variables are considered to be non-significant. The correction accounting for the autocorrelation in the noise residual is then applied to give more confidence in the coefficients determination.

## 4 Ozone variations observed by IASI

In this section, we first examine the ozone variations in IASI time series during 2008-2013 in the four layers defined in the troposphere and the stratosphere to match the IASI sensitivity (Section 2). The performance of the multiple linear model is evaluated in subsection 4.2 in terms of residuals errors, regression coefficients and associated uncertainties determined from the regression procedure (Section 3). Based on this, we characterize the principal physical processes that affect the IASI ozone records. Finally, the ability of IASI to derive apparent trends is examined in sub-section 4.3.

### 4.1 $O_3$ time series from IASI

Figure 4 (a) shows the time development of daily $O_3$ number density over the entire altitude range of the retrieved profiles based on daily medians. The time series cover the six years of available IASI observations and are separated in three 20-degree latitude belts: 30°N-50°N (top panel), 10°N-10°S (middle panel) and 30°S-50°S (bottom panel). The figure shows the well-known seasonal cycle at mid-latitudes in the troposphere and the stratosphere with maxima observed in spring-summer and in winter-spring, respectively, and a strong stability of ozone layers with time in the equatorial belt. At high latitudes of both hemispheres, the high ozone concentrations and the large amplitude of the seasonal cycle observed in MLST and UTLS are mainly the consequence of the large-scale downward poleward Brewer-Dobson circulation which is prominent in late winter below 25 km.

Figure 4 (b) presents the estimated statistical uncertainty on the $O_3$ profiles retrieved from FORLI. This total error depends on the latitude and the season, reflecting, amongst other, the

influence of signal intensity, of interfering water lines and of thermal contrast under certain conditions (e.g. temperature inversion, high thermal contrast at the surface). It usually ranges between 10 and 30% in the troposphere and in the UTLS (Upper Troposphere-Lower Stratosphere), except in the equatorial belt due to the low $O_3$ amounts (see Fig.4 (a)) which leads to larger relative errors. The retrieval errors are usually less than 5% in the stratosphere.

The relative variability (given as the standard deviation) of the daily median $O_3$ time series presented in Fig.4 (a) is shown in Fig.5, as a function of time and altitude. It is worth noting that, except in the UTLS over the equatorial band, the variability is larger than the estimated retrieval errors of the FORLI-$O_3$ data (~25% *vs* ~15% and ~10% *vs* ~5%, on average over the troposphere and the stratosphere, respectively), reflecting that the high natural temporal variability of $O_3$ in zonal bands is well captured with FORLI (Dufour et al., 2012; Hurtmans et al., 2012). The standard deviation is larger in the troposphere and in the stratosphere below 20 km where dynamic processes play an important role. The largest values (>70% principally in the northern latitudes during winter) are measured around 9-15km altitude. They highlight the influence of tropopause height variations and the STE processes. In the stratosphere, the variability is always lower than 20% and becomes negligible in the equatorial region. Interestingly, the lowest troposphere of the N.H. (below 700 hPa; <4km) is marked by an increase in both $O_3$ concentrations (Fig. 4a) and standard deviations (between ~30% and ~45%) in spring-summer, the latter being larger than the total retrieval error (less than 25%, see Fig. 4 (b)). The lower tropospheric column (e.g. ground-700 hPa) can generally not well be discriminated because of the weak sensitivity of IASI in the lowermost layers (Section 2). However, the measurements in northern mid-latitudes in spring-summer are characterized by a larger sensitivity. In the ground-700hPa columns, we find that the apriori contributions do not exceed 40% and they range between 10% and 20% over the continental regions. In addition, the stratosphere-troposphere exchanges are usually the weakest in summer. The stratospheric contributions into the IASI MLT columns are estimated to be the lowest in the summer mid-latitudes N.H. (e.g. ~35% in the 30°N-50°N band; See Fig. S5 (b) of the Supplement) and, as mentioned in Section 2, the real natural contribution originating from the troposphere reaches ~55% (cfr Fig.S6 (b) in Supplement). This certainly helps in detecting the real variability of $O_3$ in the N.H. troposphere,

and, the increase in the observed concentrations and in the variability may likely indicate a photochemical production of $O_3$ associated with anthropogenic precursor emissions (e.g. Logan et al., 1985; Fusco and Logan, 2003; Dufour et al., 2010; Cooper et al., 2010; Wilson, et al., 2012; Safieddine et al., 2013). Changes in biomass and biogenic emissions of $NO_x$, CO and non-methane organic volatile compounds (NMVOC) may also play a role. However, they only represent a small part of the total emissions for $NO_x$ and CO (e.g. ~23% *vs* 72% for the anthropogenic $NO_x$ emissions and ~40% *vs* 60% for the anthropogenic CO emissions from the emissions dataset used in the Supplement), while the biogenic emissions of NMVOC represent the largest contribution to the total (~80%).

The zonal representation of the $O_3$ variability seen by IASI is given in Fig. 6. It shows the daily number density at altitude levels corresponding to maximum of sensitivity in the four analyzed layers in most of the cases (600 hPa - ~6km; 240 hPa - ~10km; 80 hPa - ~20km; 6 hPa - ~35 km) (Section 2). The top panel (~35 km) reflects well the photochemical $O_3$ production by sunlight with the highest values in the equatorial belt during the summer (~$3x10^{12}$ molecules/$cm^3$). The middle panels (~20 km and ~10 km) shows the transport of ozone rich-air to high latitudes in late winter (up to ~$6x10^{12}$ molecules/$cm^3$ in the N.H.) which is induced by the Brewer-Dobson circulation. The fact that the patterns at ~10km are similar to those at ~20 km mainly reflects the low sensitivity of IASI to that level compared to the others. Finally, the lower panel (~6 km) presents high $O_3$ levels in spring at high latitudes (~$1.4x10^{12}$ molecules/$cm^3$ in the N.H.), which likely reflects both the STE processes and the contribution from the stratosphere due to the medium IASI sensitivity to that layer (see Section 2 and Supporting Information), and a shift from high to middle latitudes in summer which could be attributed to anthropogenic $O_3$ production. The MLT panel also reflects the seasonal oscillation of the Inter-Tropical Convergence Zone (ITCZ) around the Equator and the large fire activity in spring around 20°S-40°S.

**4.2 Multivariate regression results: Seasonal and explanatory variables**

Figure 4(a) shows superimposed on the time series of the IASI ozone concentration profile, those of the partial columns (dots) for the 4 layers (color contours). The adjusted daily time series to

these columns with the regression model defined by Eq.1 is also overlaid and shown by colored lines. The model represents reasonably well the ozone variations in the four layers, with, as illustrated for three latitude bands, good correlation coefficients (e.g. $R_{MLT}$=0.94; $R_{UTLS}$=0.91; $R_{MLT}$=0.90 and $R_{US}$=0.91 for the 30°N-50°N band) and low residuals (< 8%) in all cases. The regression model explains a large fraction of the variance in the daily IASI data over the troposphere (~85%-95%) and the stratosphere (~85%-95% in all cases, except for the UST with ~70-95%), as estimated from $\frac{\sigma\left(O_3^{Fitted\_model}(t)\right)}{\sigma\left(O_3(t)\right)}$ where σ is the standard deviation relative to the fitted regression model and to the IASI $O_3$ time series.

However, note that the fit fails to reproduce the highest ozone values (>5x$10^{12}$ molecules/$cm^3$) above the seasonal maxima for the 30°N-50°N latitude band, especially in the MLST during the springs 2009 and 2010. This could be associated with occasional downward transport of upper atmospheric $NO_x$-rich air occurring in winter and spring at high latitudes (Brohede et al., 2008) following the strong subsidence within the intense Arctic vortex in 2009-2010 (Pitts et al., 2011) or with the missing time-lags in the regression model between the QBO and ENSO variables and the response of mid-latitude lower stratospheric ozone (Neu et al., 2014).

Fig.7 displays the annual cycle averaged over the 6 years recorded by IASI (dots) for the studied layers and bands, as well as that from the fit of the daily $O_3$ columns (lines). The regression model follows perfectly the $O_3$ variations in terms of timing of $O_3$ maxima and of amplitude of the cycle. The fit is generally characterized by low residuals (<10%) and good correlation coefficients (0.70-0.95), which indicates that the regression model is suitable to describe the zonal variations. Exception is found over the Southern latitudes (residual up to 15% and R down to 0.61) probably because of the variation induced by the ozone hole formation which is not parameterized in the regression model, and because of the low temporal sampling of daytime IASI measurements in this region.

From Figure 7, the following general patterns in the $O_3$ seasonal cycle can be isolated from the zonally averaged IASI datasets:

1- In UST (top left panel), the maxima is in the equatorial belt, around $4.7x10^{18}$ molecules/$cm^2$ throughout the year and the amplitudes are small compared to the averaged $O_3$ values. The largest amplitude in the annual cycle is found in the N.H. between 30N and 50N where $O_3$ peaks in July after the highest solar elevation (in June) following a progressive buildup during spring-summer. In agreement with FTIR observations (e.g. Steinbrecht et al., 2006; Vigouroux et al., 2008), a shift of the $O_3$ maximum from spring (March-April) to late summer (August-September) is found as one moves from high to low latitudes in the N.H. In the S.H., the general shape of the annual cycle which shows a peak in October-November before the highest solar elevation (in December), results from loss mechanisms depending on the annual cycle of temperatures and other trace gases. Other effects such as changing Brewer-Dobson circulation, light absorption and tropical stratopause oscillations may also considerably impact the cycle in this layer (Brasseur and Solomon, 1984; Schneider et al., 2005).

2- In the lower stratosphere (MLST and UTLS, top right and bottom left panels), the pronounced amplitudes of the annual cycle is dominated by the influence of the Brewer Dobson circulation with the highest $O_3$ values observed over polar regions (reaching ~$6x10^{18}$ molecules/$cm^2$ on average *vs* ~$2x10^{18}$ molecules/$cm^2$ on average in the equatorial belt). The maximum is shifted from late winter at high latitudes to spring at lower latitudes.

3- In MLT (bottom right panel), we clearly see a large hemispheric difference with the highest values over the N.H. (also in UTLS). Maxima are observed in spring, reflecting more effective STE processes. A particularly broad maximum from spring to late summer is observed in the 30N-50N band. It probably points to anthropogenic production of $O_3$. This has been further investigated in the Supplement through MOZART4-IASI comparison by using constant anthropogenic emissions in the model settings (see Fig. S2). The results show clear differences between the modeled and the observed MLT seasonal cycles, which highlights the need for further investigation of the role of anthropogenically produced $O_3$ and the realism of anthropogenic emissions inventories.

Figure 8 presents all the fitted regression parameters included in Eq. 1 (Section 3) in the four layers as a function of latitude. The uncertainty in the 95% confidence limits which accounts for

the autocorrelation in the noise residual is given by error bars. The constant term (Fig.8a) is found to be statistically significant (uncertainty<10%) in all cases. It captures the two ozone maxima in the stratosphere: one over the Northern Polar regions in the MLST and one at equatorial latitudes in the UST (~4.5 x$10^{18}$ molecules/$cm^2$), the important decrease of $O_3$ in the lower stratospheric layers (UTLS and MLST) moving from high to equatorial latitudes, and the weak negative and strong positive gradients in the Northern MLT and in the UST, respectively. The sum of the constant terms of the four layers varies between 7.50x$10^{18}$ (equatorial region) and 9.50x$10^{18}$ molecules/$cm^2$ (polar regions) and is similar to the one of the fitted total column (relative differences < 3.5%) (red line). Note that the constant terms in the UTLS region in the mid-latitudes and in the tropics are certainly affected by the fact that the FORLI-$O_3$ profiles are biased high by ~10-15% in this layer and latitude bands (Dufour et al., 2012; Gazeaux et al., 2012). The representativeness of the 20-degree zonal averages in terms of spatial variability has been examined by fitting the IASI time series for specific locations in the N.H. (results shown with stars in Fig.8a): the constant terms are found to be consistent, within their uncertainties, with those averaged per latitude bands in all cases. Over the polar region where $O_3$ shows a large natural variability, the regression coefficient is characterized by a large uncertainty.

The regression coefficients for other variables (harmonic and proxy terms) which are retained in the regression model by the stepwise elimination procedure are shown in Fig.8 (b). They are scaled by the fitted constant term and the error bars represent the uncertainty in the 95% confidence limits accounting for the autocorrelation in the noise residual. A positive (or negative) sign of the coefficients indicates that the associated variables are correlated (or anti-correlated) with the IASI $O_3$ time series. Note that if the uncertainty is larger than its associated estimate (i.e. larger than 100%, corresponding to an error bar overlapping the zero line), it means that the estimate becomes statistically non-significant when accounting for the autocorrelation in the noise residuals at the end of the elimination process. This is summarized in Table S1 of the Supplement. The contribution of the fitted variables into the IASI $O_3$ variations is estimated as $\frac{\sigma\left(\left[a_n; b_n; x_j\right]\left[\cos(n\omega t); \sin(n\omega t); X_{norm,j}\right]\right)}{\sigma\left(O_3(t)\right)}$ where σ is the standard deviation relative to the fitted signal of harmonic or proxy terms and to the IASI $O_3$ time series. From Figure 8, we find that:

1- The annual harmonic term (upper left) is the main driver of the $O_3$ variability and largely dominates (scaled $a_1+b_1$ around ± 40%) over the semi-annual one (upper right; scaled $a_{2+}b_2$ around ± 15%). In UTLS and MLST, its amplitude decreases from high to low latitudes likely following the cycle induced by the Brewer-Dobson circulation (*cfr.* Fig.6 and Fig.7) and the sign of the coefficient accounts for the winter-spring maxima in both hemispheres (negative values in the S.H. and positive ones in the N.H). The annual term contributes importantly around 45%-85% of the observed $O_3$ variations, except in the 10°N-30°N and equatorial bands (10%-30%), while the influence of the semi-annual variation on $O_3$ is smaller (10%-25%) and highly variable between the bands. In the UST, the amplitudes vary only slightly (around -5% to 5%) and account for the weak summer maximum. The contributions of the annual harmonic term are estimated between 5%-30%. As expected, the uncertainties associated with the annual terms are very weak and most of the harmonic terms (annual and seasonal) are statistically significant.

2- The QBO and solar flux proxies are generally minor (scaled coefficients <10% and contributions <15%) and they are often statistically non-significant contributors to $O_3$ variations after accounting for the autocorrelation in the noise residual (see Table S1 in the Supplement), except in equatorial region (scaled coefficients of 10-15% in UTLS and contributions up to 75% and 21% for QBO and SF, respectively) where they are important drivers of $O_3$ variations (e.g. Logan et al., 2003; Steinbrecht et al., 2006b; Soukharev and Hood, 2006; Fadnavis and Beig, 2009). Previous studies have indeed supported the solar influence on the lower stratospheric equatorial dynamics (e.g. Soukharev and Hood, 2006; McCormack et al., 2007). Note that the $QBO^{30}$ proxy (data not shown) has negative coefficients for the mid-latitudes, which is in line with Frossard et al. (2013).

3- The contributions described by the ENSO and NAO/AAO proxies are generally very weak (<10% and <5%, respectively), with scaled coefficients lower than 5%, and, in many cases for the NAO/AAO proxies, they are even not statistically significant when taking into account the correlation in the noise residuals (see Table S1 in Supplement). Despite of this, it is worth pointing out that their effects on the $O_3$ variations are comparable to the results published in the previous studies. The negative ENSO coefficient in the tropical UTLS is consistent with results from Neu et al. (2014). Rieder et al. (2013) and Frossard et al. (2013)

have also shown large regions of negative coefficients for NAO North of 40°N, and large regions of positive and negative coefficient estimates for ENSO, North of 30°N and South of 30°S, respectively.

We note that the non-representation of time-lags in the proxy time series may be underestimating the role of some geophysical variables on $O_3$ variations, in particular that of ENSO and QBO in zonal bands outside the regions where these geophysical quantities are measured (i.e. Niño region 3.4 for ENSO and Singapore for QBO). Finally, we see in Fig.8 (b), large uncertainties associated with the regression coefficients in UTLS in comparison with other layers, and in polar regions in comparisons with other bands. We interpret this as an effect from the high natural variability of $O_3$ measured by IASI in UTLS (see Fig.5) and from missing parameterizations and low temporal sampling of daytime IASI measurements over the poles, respectively.

As a general feature, the results demonstrate the representativeness of the fitted models in each layer and latitude band. This good performance of the regression procedure allows examination of the adjusted linear trend term in Section 4.3 below.

### 4.3 Multivariate regression results: trend over 2008-2013

An additional goal of the multivariate regression method applied to the IASI $O_3$ time series is to determine the linear trend term and its associated uncertainty. Despite the fact that more than 10 years of observations, corresponding to the large scale of solar cycle, is usually required to perform such a trend analysis, we could argue that statistically relevant trends could possibly be derived from the first six years of IASI observations, owing to the high spatio-temporal frequency (daily) of IASI global observations, to the daily "fingerprint" in the solar flux (see Figure 3 (a)), possibly making it distinguishable from a linear trend, and to its weak contribution to $O_3$ variations (see section 4.2. and references therein). To verify the specific advantage of IASI in terms of frequency sampling, we compare, in the subsections below, the statistical relevance of the trends when retrieved from the monthly averaged IASI datasets *vs* the daily averages as above, in the 20° zonal bands for the 4 partial and the total columns.

#### 4.3.1. Regressions applied on daily *vs* monthly averages

Figure 9 (top) provides, as an example, the 6-year time series of IASI $O_3$ daily averages (left panels) compared to the monthly averages (right panels) for the 30°S-50°S latitude band in the UST (dark blue), along with the results from the regression procedure (light blue). Note that either daily or monthly F10.7, NAO and AAO proxies (see Table 1) are used depending on the frequency of the IASI $O_3$ averages to be adjusted. The second row in Fig.9 provides the deseasonalised IASI and fitted time series, calculated by subtracting the model seasonal cycle from the time series, as well as the residuals (red curves). The averaged residuals relative to the deseasonalised IASI time series strongly vary with the layers and latitudinal bands and usually range between 30% and 60%. The fitted signal in DU of each proxy is shown on the bottom panels. The $O_3$ time series and the solar flux signal resulting from the adjustment without the linear term trend in the regression model are also represented (orange lines in $2^d$ and bottom panels, respectively). When it is not included in the regression model, the linear trend term is only partly compensated by the solar flux term in the daily averages. This leads to an offset between the fitted $O_3$ time series resulting from the both regression models (with and without the linear term), which corresponds well to a trend over the IASI period, and, consequently, to larger residuals (e.g. 80% without *vs* 44% with the linear term for this example and 94% without *vs* 58% with the linear trend term for the 30°S-50°S band in the MLST illustrated in Fig. S1 of the Supplement). This offset is observed for a lot of layers and latitudinal bands. On the contrary, the linear term can largely be compensated by the solar flux term in the monthly averages: the offset is weak and the relative difference between the both fitted models is smaller (averaged differences relative to the deseasonalised IASI time series of10% in monthly data *vs* 17% in daily data for this example). In this example, the linear and solar flux terms are even not simultaneously retained in the iterative stepwise backward procedure when applied on the monthly averages while they are when applied on daily averages. This effective co-linearity of the linear and the monthly solar flux terms translates to larger model fit residuals (44% in daily averages *vs* 60% in monthly averages in UST, relative to the deseasonalised IASI time series), to smaller relative differences between both regression models (with and without the linear term) (17% in daily vs 10% in monthly data), and to larger uncertainty on the trend coefficients when using the monthly data in comparison with the daily data. This even leads, in this specific

example, to a not statistically significant linear term of 1.21±1.30DU/yr when derived from monthly averages *vs* a significant trend of 1.74±0.77DU/yr from daily averages.

The same conclusions can be drawn from the fits in other layers and latitude bands, especially those where the solar cycle variation of ozone is large (MLST and UTLS) or where the ozone recovery occurs (UST). A larger trend uncertainty associated with monthly data *vs* daily data is found in all situations (see Table 2, Section 4.3.2 below).

This brings us to the important conclusion that, thanks to the unprecedented sampling of IASI, apparent trends can be detected in FORLI-$O_3$ time series even on a short period of measurements. This supports the need for regular and high frequency measurements for observing ozone variations underlined in other studies (e.g. Saunois et al., 2012). The $O_3$ trends from the daily averages of IASI measurements are discussed and compared with results from the monthly averages in the subsection below.

#### 4.3.2. $O_3$ trends from daily averages

Table 2 summarizes the trends and their uncertainties in the 95% confidence limit, calculated for each 20° zonal band and for the 4 partial and the total columns. In the northern and southern polar regions, the polar night period is not covered because only IASI observations during sunlight (over Feb-Oct and Oct-Apr for N.H. and S.H., respectively) are used in this study (See Section 2). For the sake of comparison, the trends are reported for both the daily (top values) and the monthly (bottom values) averages, and their uncertainties account for the auto-correlation in the noise residuals considering a time lag of 1-day or 1-month, respectively. We show that the daily and monthly trends in all layers and all latitude bands fall within each other uncertainties, but that the use of daily median strongly helps in reducing everywhere the uncertainty associated with the trends for the reasons discussed above (Section 4.3.1). This is particularly observed in the UST where the ozone hole recovery would occur, but also in the MLST and the UTLS where the solar cycle variation of ozone is the largest (see Figure 8). As a consequence, the UST trends in monthly averages are shown to be mostly non-significant in comparison with those from daily

averages. Table 3 summarizes the trends in the daily averages for two 3-month periods: June-July-August (JJA) and December-January-February (DJF).

From Tables 2 and 3, we observe very different trends according to the latitude and the altitude. From Table 2, we find for the total columns that the trends derived from the daily medians are only significant at high northern latitudes and that they are interestingly of the same order as those obtained from other satellites and assimilated satellite data (Weatherhead and Anderson, 2006; Knibbe et al., 2014) or from ground-based measurements (Vigouroux et al., 2008) calculated over longer time periods. The non-significant trends calculated for the mid- and low latitudes of the N.H. are also comparable to the results published in the previous studies (Reinsel et al., 2005; Andersen et al., 2006a; Vigouroux et al., 2008). Regarding the individual layers, we find the following:

1- In the US, significant positive trends are observed in both hemispheres from the daily medians, particularly over the mid- and high latitudes of both hemispheres (e.g. 1.74±0.77 DU/yr in the 30°S-50°S band, i.e., 12%/decade) where the changes in ozone trends before and after the turnaround in 1997 have been found to be the highest. Kÿrola et al. (2013) and Laine et al. (2014) report for instance a change of up to 10%/decade in $O_3$ trends between 1997-2011 *vs* 1984-1997. Positive trends in the UST are consistent with many previous observations if one considers the fact that the period covered by IASI is later than those reported in previous studies and that the recovery rate seems to increase since the beginning of the turnaround (Knibbe et al. (2014) reports a factor of two increase in the recovery rate between 1997-2010 with ~0.7DU/yr and 2001-2010 with ~1.4DU/yr in the S.H.). They could indicate a leveling off of the negative trends that were observed since the second half of the 1990's mostly from satellites and ground-based monthly mean data (e.g. WMO 2006, 2011; Randel and Wu, 2007; Vigouroux et al., 2008; Steinbrecht et al., 2009; Jones et al., 2009; McLinden et al., 2009; Laine et al. 2014; Nair et al., 2014). The causes of this "turnaround" remain, however, uncertain. If the compensating impact of decreasing chlorine in recent years and maximum solar cycle (over 2011-2012 in the period studied here) is probably part of the answer (e.g. Steinbrecht et al., 2004), the effects of changing stratospheric temperatures and Brewer-Dobson circulation (Salby et al., 2002; Reinsel et al., 2005;

Dhomse et al., 2006; Manney et al., 2006) could also contribute and should be further investigated. The long-lasting cold winter/spring 2011 in the Arctic leading to unprecedented ozone loss (Manney et al., 2011), could explain the non-significant trend in the 70°N-90°N band. This is supported by the results in winter (Table 3). From Table 3, we generally find significant positive trends in summer N.H. and weaker positive or even non-significant trends in winter S.H. A non-significant trend is also calculated for the 70°S-90°S band in spring (data not shown). This could indicate the strong influence of changing stratospheric temperatures on ozone depletion from year to year (e.g. Dhomse et al., 2006), leading to larger uncertainties in our trends estimations and larger fitting residuals (see Section 4.2) due to the fact that the stratospheric temperature is not taken into account as an explanatory variable in the model.

2- In the MLST, one can see that, except in the high latitude bands, the trends are either non-significant or significantly negative. This is in agreement with the trend analysis of Jones et al. (2009) for the 20-25 km altitude range over the 1997-2008 period, as well as with other studies at N.H. latitudes, which investigated $O_3$ changes in the 18-25 km range between 1996 and 2005 (Miller et al., 2006; Yang et al., 2006; Kivi et al., 2007). The results derived separately for summer and winter in Table 3 are also in line with those of Kivi et al. (2007) which reported contrasted trends in the Arctic MLST depending on season.

3- In the UTLS, negative trends are calculated in the tropics and significant positive trends are found in the mid- and high latitudes of N.H., these latter falling within the uncertainties of those reported by Kivi et al. (2007) for the tropopause-150 hPa layer between 1996 and 2003. The large positive trends calculated at Northern latitudes (e.g. 1.28±0.82 DU/year in the 70°N-90°N band) contribute for ~ 30 % to the positive trend for the total column. This result is consistent with Yang et al. (2006) which reported that UTLS contributes 50% to positive trends for the total columns measured in the mid-latitudes of the N.H. from ozonesondes. In that study, these positive trends were linked to changes in atmospheric dynamics either related to natural variability induced by potential vorticity and tropopause height variations or related to anthropogenic climate change. Hence, the apparent increase in total ozone in the mid-latitudes of the N.H. seen by IASI would reflect the combined contribution of dynamical variability and declining ozone-depleting substances (e.g. Weatherhead and Andersen, 2006;

WMO, 2006; Harris et al., 2008, Nair et al., 2014). It is worth to keep in mind that these effects are not independently accounted for in the regression model. Previous studies reported, however, that dynamical and chemical processes are physically coupled in the atmosphere, making difficult to define unambiguously such drivers in a statistical model (e.g. Mäder et al., 2007; Harris et al., 2008). On a seasonal basis (see Table 3), the trends seen by IASI at Northern latitudes in summer are all significantly positive and increasing towards the pole. Note that the trends in upper layers may contribute to the ones calculated in UTLS due to the medium IASI sensitivity to that layer (*cfr*. Section 2).

4- In the MLT, most of the trends are significantly negative (Tables 2 and 3). The non-significant trends in polar regions could be partly related to the lack of IASI sensitivity to tropospheric $O_3$ (see Section 2, Fig.2). On a seasonal basis, we see that the negative trends are more pronounced during the JJA period (around -0.25±0.10DU/yr) for all bands except between 30°N and 10°S. In the N.H., these results tend to confirm the leveling off of tropospheric ozone observed in recent years during the summer months (Logan et al., 2012). This trend, however, remains difficult to interpret because it could be linked to a variety of processes including most importantly: the decline of anthropogenic emissions of ozone precursors, the increase of UV-induced $O_3$ destruction in the troposphere and STE processes (Isaksen et al., 2005; Logan et al., 2012; Parrish et al., 2012; Hess and Zbinden, 2013). As a consequence, it is hard to reconcile the trends in tropospheric ozone with changes in emissions of ozone precursors. However, trends in emissions have already been able to qualitatively explain measured ozone trends over some regions but with inconsistent magnitude between observations and model simulations (e.g. Cooper et al., 2010; Logan et al., 2012; Wilson et al., 2012). It is also worth to keep in mind that due to medium sensitivity of IASI to the troposphere, the a priori contribution and ozone variations in stratospheric layers may largely influence the trends seen by IASI in the MLT layer (*cfr*. Section 2 and Supporting Information).

#### 4.3.3. $O_3$ trends from IASI *vs* FTIR data

In order to validate the trends inferred from IASI in the UST and in the total columns, we compare them with those obtained from ground-based FTIR measurements at several NDACC

679 stations (Network for the Detection of Atmospheric Composition Change, available at
680 http://www.ndsc.ncep.noaa.gov/data/data_tbl/) by using the same fitting procedure and taking
681 into account the autocorrelation in the noise residuals. A box of 1°x1° centered on the stations
682 has been used for the collocation criterion. The regression model is applied on the daily FTIR
683 data for a series of time periods starting after the turnaround point (from 1998 for mid-latitude
684 stations and from 2000 for polar stations), as well as for the same periods as recently studied in
685 Vigouroux et al. (2014) for the sake of comparison. Note that because we are not interested here
686 in validating the IASI columns which was achieved in previous papers (e.g. Dufour et al., 2014;
687 Oetjen et al., 2014) but in validating the trends obtained from IASI, we did not correct biases
688 between IASI and FTIR due to different vertical sensitivity and *a priori* information. The results
689 are given in DU/year in Table 4. We see large significant positive total column trends from IASI
690 at middle and polar stations (e.g. 5.26±4.72 DU/yr at Ny-Alesund), especially during spring.
691 These values are consistent with those reported in Knibbe et al. (2014) for the 2001-2010 period
692 in spring in the Antarctic (around 3-5DU/yr). This trend is not obtained from the FTIR data for
693 which trends are found to be mostly non-significant (even not retained in the stepwise
694 elimination procedure in some cases) as reported in Vigouroux et al. (2014), except at
695 Jungfraujoch which shows a trend of 5.28±4.82DU/yr over the 2008–2012 period. For the
696 periods starting before 2000, we calculated from FTIR, in agreement with Vigouroux et al.
697 (2014), a significantly negative trend at Ny-Alesund for the total column and significantly
698 positive trends at polar stations for the US. In addition, we see from Table 4 a leveling off of $O_3$
699 at polar stations in the UST after 2003, as previously reported in Vigouroux et al. (2014), which
700 was explained by a compensation effect between the decrease of solar cycle after its maximum in
701 2001-2002 and a positive trend. These trends are, however, non-significant and inferred only
702 from few FTIR measurements (see Number of days column, Table 4).
703
704 From IASI, it is worth to point out that, in all cases, positive trends are calculated in the UST
705 (even if some are not significant) and that these trends are consistent with those calculated from
706 FTIR data covering a ~11-year period and starting after the turnaround (e.g. at Thule;
707 1.24±1.09DU/yr from IASI for the period 2008-2013 *vs* 1.42±0.78DU/yr from the FTIR over
708 2001-2012). This is illustrated for three stations (Ny-Alesund, Thule and Kiruna) in Fig.10 which

compares the time series from IASI (2008-2013, in red) with those from FTIR covering periods starting after the turnaround (in blue). Their associated trends as well as the trend calculated from FTIR covering the IASI period (in green) are also indicated.

In order to better characterize the effect of the temporal frequency on determining statistical trends, the IASI time series have been subsampled to match the temporal resolution of FTIR. The associated trend values are also indicated in Table 4 ($2^d$ row). In any cases, we observe that the fitted trends inferred from both IASI and FTIR with the same temporal samplings are within the uncertainties of each other and that those associated with the subsampled IASI datasets are significantly larger than those obtained with the daily ones, leading to statistically non-significant trends.

Even if validating the IASI fitted trends with independent datasets is challenging due to the short-time period of available IASI measurements and the insufficient number of usable correlative measurements over such a short period, the results obtained for IASI *vs* FTIR tend to confirm the conclusion drawn in subsections 4.3.1 and 4.3.2, that the high temporal sampling of IASI provides good confidence in the determination of the trends even on periods shorter than those usually required from other observational means.

## 6 Summary and conclusions

In this study, we have analyzed 6 years of IASI $O_3$ profile measurements as well as the total $O_3$ columns based on the profile. Four layers have been defined following the ability of IASI to provide reasonably independent information on the ozone partial columns: the mid-lower troposphere (MLT), the upper troposphere – lower stratosphere (UTLS), the mid-lower stratosphere (MLST) and the upper stratosphere (UST). Based on daily values of these four partial or of the total columns in 20-degree zonal averages, we have demonstrated the capability of IASI for capturing large scale ozone variability (seasonal cycles and trends) in these different layers. We have presented daytime vertical and latitudinal distributions for $O_3$ as well as their evolution with time and we have examined the underlying dynamical or chemical processes. The distributions were found to be controlled by photochemical production leading to a maximum in

summer at equatorial region in the UST, while they reflect the impact of the Brewer-Dobson circulation with maximum in winter-spring at mid- and high latitude in the MLST and in the troposphere. The effect of the photochemical production of $O_3$ from anthropogenic precursor emissions was also observed in the troposphere with a shift in the timing of the maximum from spring to summer in the mid-latitudes of the N.H.

The dynamical and chemical contributions contained in the daily time development of IASI $O_3$ have been analyzed by fitting the time series in each layer and for the total column with a set of parameterized geophysical variables, a constant factor and a linear trend term. The model was shown to perform well in term of residuals (<10%), correlation coefficients (between 0.70 and 0.99) and statistical uncertainties (<7%) for each fitted proxies. The annual harmonic terms (seasonal behavior) were found to be largely dominant in all layers but the US, with fitted amplitudes decreasing from high to low latitudes in agreement with the Brewer-Dobson circulation. The QBO and solar flux terms were calculated to be important only in the equatorial region, while other dynamical proxies accounted for in the regression (ENSO, NAO, AAO) were found negligible.

Despite the short time period of available IASI dataset used in this study (2008-2013) and the potential ambiguity between the solar and the linear trend terms, statistically significant trends were derived from the six first years of daily $O_3$ partial columns measurements (on the contrary to monthly averages which lead to mostly non-significant trends). This result which was strengthened from comparisons with the regression applied on local FTIR measurements, is remarkable as it demonstrates the added value of IASI exceptional frequency sampling for monitoring medium to long-term changes in global ozone concentrations. We found two important apparent trends:

1) Significant positive trends in the upper stratosphere, especially at high latitudes in both hemispheres (e.g. 1.74±0.77DU/yr in the 30°S-50°S band), which are consistent with a probable "turnaround" for upper stratospheric $O_3$ recovery (even if the causes of such a turnaround are still under investigations). In addition, the trends calculated for some local stations are in line with those calculated from FTIR measurements after the turnaround.

2) Negative trends in the troposphere at mid- and high Northern latitudes, especially during summer (e.g. -0.26±0.11DU/yr in the 30°N-50°N band) which are in line with the decline of ozone precursor emissions.

To confirm the above findings beyond the 6 first years of IASI measurements and to better disentangle the effects of dynamical changes, of the 11-year solar cycle and of the equivalent effective stratospheric chlorine (EESC) decline on the $O_3$ time series, further years of IASI observations will be required, and more complete fitting procedures (including, among others, proxies to account for the decadal trend in the EESC, for the ozone hole formation, for changes in the Brewer-Dobson circulation, as well as including time lags in ENSO and QBO proxies) will have to be explored. Further investigation on the regressors uncertainties and on the total error on ozone measurements should be performed as well to understand on the unexplained variations in IASI $O_3$ records.

This will be achievable with the long-term homogeneous records obtained by merging measurements from the three successive IASI instruments on MetOp-A (2006); -B (2012) and –C (2018), and by IASI successor on EPS-SG after 2021 (Clerbaux and Crevoisier, 2013; Crevoisier et al., 2014).

**Acknowledgments**

IASI has been developed and built under the responsibility of the Centre National d'Etudes Spatiales (CNES, France). It is flown onboard the MetOp satellites as part of the EUMETSAT Polar System. The IASI L1 data are received through the EUMETCast near real time data distribution service. Ozone data used in this paper are freely available upon request to the corresponding author. We acknowledge support from the $O_3$-CCI project funded by ESA and by the O3M-SAF project funded by EUMETSAT. P.-F. Coheur and C. Wespes are, respectively, Senior Research Associate and Postdoctoral Researcher with F.R.S.-FNRS. The research in Belgium was also funded by the Belgian State Federal Office for Scientific, Technical and Cultural Affairs and the European Space Agency (ESA Prodex IASI Flow and $BO_3$MSAF). The National Center for Atmospheric Research is funded by the National Science Foundation.

## References


Andersen, S. B. and Knudsen, B. M.: The influence of polar vortex ozone depletion on NH mid-latitude ozone trends in spring, Atmos. Chem. Phys., 6, 2837–2845, 2006a.

Andersen, S. B., Weatherhead, E. C., Stevermer, A., Austin, J., Brühl, C, Fleming, E. L., de Grandpré, J., Grewe, V., Isaksen, I., Pitari, G., Portmann, R. W., Rognerud, B., Rosenfield, J. E., Smyshlyaev, S., Nagashima, T., Velders, G. J. M., Weisenstein, D. K., and Xia, K.: Comparison of recent modeled and observed trends in total column ozone, J. Geophys. Res., 111, D02303, doi:10.1029/2005JD006091, 2006b.

Anton, M., D. Loyola, C. Clerbaux, M. Lopez, J. Vilaplana, M. Banon, J. Hadji-Lazaro, P. Valks, N. Hao, W. Zimmer, P. Coheur, D. Hurtmans, and L. Alados-Arboledas: Validation of the Metop-A total ozone data from GOME-2 and IASI using reference ground-based measurements at the Iberian peninsula, Remote Sensing of Environment, 115, 1380-1386, 2011.

August, T., D. Klaes, P. Schlüssel, T. Hultberg, M. Crapeau, A. Arriaga, A., O'Carroll, A., Coppens, D., Munro, R., Calbet, X.: IASI on Metop-A: Operational Level 2 retrievals after five years in orbit. Journal of Quantitative Spectroscopy and Radiative Transfer, 114(11), 1340–1371, 2012.

Barret, B., Le Flochmoen, E., Sauvage, B., Pavelin, E., Matricardi, M., and Cammas, J. P.: The detection of post-monsoon tropospheric ozone variability over south Asia using IASI data, Atmos. Chem. Phys., 11, 9533-9548, doi:10.5194/acp-11-9533-2011, 2011.

Bourassa, A. E., D. A. Degenstein, W. J. Randel, J. M. Zawodny, E. Kyrölä, C. A. McLinden, C. E. Sioris, and C. Z. Roth: Trends in stratospheric ozone derived from merged SAGE II and Odin-OSIRIS satellite observations, Atmos. Chem. Phys., 14, 6983–6994, doi:10.5194/acp-14-6983-2014, 2014.

Boynard, A., C. Clerbaux, P.-F. Coheur, D. Hurtmans, S. Turquety, M. George, J. Hadji-Lazaro, C. Keim, and J. Meyer-Arnek: Measurements of total and tropospheric ozone from IASI: comparison with correlative satellite, ground-based and ozonesonde observations, Atmos. Chem. Phys., 9, 6255-6271, 2009.

Brohede, S., McLinden, C. A., Urban, J., Haley, C. S., Jonsson, A. I., and Murtagh, D.: Odin stratospheric proxy NOy measurements and climatology, Atmos. Chem. Phys., 8, 5731–5754, doi:10.5194/acp-8-5731 2008, 2008.

Brasseur, G. and Solomon, S: Aeronomy of the Middle Atmosphere, 441 pp., D. Reidel Publishing Company, Dordrecht, The Netherlands, 1984.

Chipperfield, M. P., Kinnersley, J. S., and Zawodny, J.: A two-dimensional model study of the QBO signal in SAGE II $NO_2$ and $O_3$, Geophys. Res. Lett., 21, 589–592, 1994.

Chipperfield, M. P.: A three-dimensional model study of longterm mid-high latitude lower stratosphere ozone changes, Atmos. Chem. Phys., 3, 1253–1265, 2003.

Clarisse L., D. Hurtmans, C. Clerbaux, J. Hadji-Lazaro, Y. Ngadi, P.-F. Coheur: Retrieval of sulphur dioxide from the infrared atmospheric sounding interferometer (IASI) Atmospheric Measurement Techniques 5, 3, 581-594, 2012.

Clerbaux, C., A. Boynard, L. Clarisse, M. George, J. Hadji-Lazaro, H. Herbin, D. Hurtmans, M. Pommier, A. Razavi, S. Turquety, C. Wespes, and P.-F. Coheur: Monitoring of atmospheric composition using the thermal infrared IASI/MetOp sounder, Atmos. Chem. Phys., 9, 6041-6054, 2009.

Clerbaux C. and C. Crevoisier: New Directions: Infrared remote sensing of the troposphere from satellite: Less, but better, Atmospheric Environment, 72, 24-26, 2013.

Coheur, P.-F., B. Barret, S. Turquety, D. Hurtmans, J. Hadji-Lazaro, and C. Clerbaux: Retrieval and characterization of ozone vertical profiles from a thermal infrared nadir sounder, J. Geophys. Res., 110, D24, 303, doi:10.1029/2005JD005845, 2005.

Cooper, O., Parrish, D., Stohl, A., Trainer, M., Nédélec, P., Thouret, V., Cammas, J., Oltmans, S., Johnson, B., and Tarasick, D.: Increasing springtime ozone mixing ratios in the free troposphere over western North America, Nature, 463, 344–348, doi:10.1038/nature08708, 2010.

Crevoisier, C., Clerbaux, C., Guidard, V., Phulpin, T., Armante, R., Barret, B., Camy-Peyret, C., Chaboureau, J.-P., Coheur, P.-F., Crépeau, L., Dufour, G., Labonnote, L., Lavanant, L., Hadji-Lazaro, J., Herbin, H., Jacquinet-Husson, N., Payan, S., Péquignot, E., Pierangelo, C., Sellitto, P., and Stubenrauch, C. : Towards IASI-New Generation (IASI-NG): impact of improved spectral resolution and radiometric noise on the retrieval of thermodynamic, chemistry and climate variables, Atmos. Meas. Tech., 7, 4367-4385, 2014.

de Laat, A. T. J., R. J. van der A, and M. van Weele: Tracing the second stage of ozone recovery in the Antarctic ozone-hole with a “big data” approach to multivariate regressions, Atmos. Chem. Phys.,15, 79–97, doi:10.5194/acp-15-79-2015, 2015.

863 Dhomse, S., Weber, M., Wohltmann, I., Rex, M., and Burrows, J. P.: On the possible causes of
864 recent increases in northern hemispheric total ozone from a statistical analysis of satellite data
865 from 1979 to 2003, Atmos. Chem. Phys., 6, 1165–1180, doi:10.5194/acp-6-1165-2006, 2006.
866 Dufour, G., M. Eremenko, J. Orphal, and J.-M. Flaud: IASI observations of seasonal and day-to-
867 day variations of tropospheric ozone over three highly populated areas of China: Beijing,
868 Shanghai, and Hong Kong, Atmos. Chem. Phys., 10, 3787-3801, 2010.
869 Dufour, G., M. Eremenko, A. Griesfeller, B. Barret, E. LeFlochmoen, C. Clerbaux, J. Hadji-
870 Lazaro, P.-F. Coheur, and D. Hurtmans: Validation of three different scientific ozone products
871 retrieved from IASI spectra using ozonesondes, Atmos. Meas. Tech., 5, 611-630, 2012.
872 Fadnavis, S. and Beig, J.: Quasibiennial Oscillation in Ozone and Temperature over Tropics, J.
873 Atmos. Sol. Terr. Phys., 71, 1450–1455, doi:10.1016/j.jastp.2008.11.012, 2009.
874 Gardiner, T., Forbes, A., de Mazière, M., Vigouroux, C., Mahieu, E., Demoulin, P., Velazco, V.,
875 Notholt, J., Blumenstock, T., Hase, F., Kramer, I., Sussmann, R., Stremme,W., Mellqvist, J.,
876 Strandberg, A., Ellingsen, K., and Gauss, M.: Trend analysis of greenhouse gases over Europe
877 measured by a network of ground-based remote FTIR instruments, Atmos. Chem. Phys., 8,
878 6719–6727, 2008.
879 Frossard, L., H.E. Rieder, M. Ribatet, J. Staehelin, J. A, Maeder, S. Di Rocco, A. C. Davison, T.
880 Pete.: On the relationship between total ozone and atmospheric dynamics and chemistry at mid-
881 latitudes – Part 1: Statistical models and spatial fingerprints of atmospheric dynamics and
882 chemistry, Atmos. Chem. Phys., 13, 147–164, doi:10.5194/acp-13-147-2013, 2013.
883 Fusco, A. C. and Logan, J. A., Analysis of 1970–1995 trends in tropospheric ozone at Northern
884 Hemisphere midlatitudes with the GEOS-CHEM model, J. Geophys. Res., 108, 4449,
885 doi:10.1029/2002JD002742, 2003.
886 Gazeaux, J., C. Clerbaux, M. George, J. Hadji-Lazaro, J. Kuttippurath, P.-F. Coheur, D.
887 Hurtmans, T. Deshler, M. Kovilakam, P. Campbell, V. Guidard, F. Rabier, and J.-N. Thepaut:
888 Intercomparison of polar ozone profiles by IASI/Metop sounder with 2010 concordiasi
889 ozonesonde observations, Atmos. Meas. Tech., 5, 7923-7944, 2012.
890 Hadjinicolaou, P., Pyle, J. A., and Harris, N. R. P.: The recent turnaround in stratospheric ozone
891 over northern middle latitudes: A dynamical modeling perspective, Geophys. Res. Lett., 32,
892 L12821, doi:10.1029/2005GL022476, 2005.

Harris, N. R. P., E. Kyrö, J. Staehelin, D. Brunner, S.-B. Andersen, S. Godin-Beekmann, S., Dhomse, P. Hadjinicolaou, G. Hansen, I. Isaksen, A. Jrrar, A. Karpetchko, R. Kivi, B. Knudsen, P. Krizan, J. Lastovicka, J. Maeder, Y. Orsolini, J. A. Pyle, M. Rex, K. Vanicek, M. Weber, I. Wohltmann, P. Zanis and C. Zerefos: Ozone trends at northern mid- and high latitudes – a European perspective. *Ann. Geophys*., 26, 1207-1220, 2008.

Hauchecorne, A., Bertaux, J. L., Dalaudier, F., Keckhut, P., Lemennais, P., Bekki, S., Marchand, M., Lebrun, J. C., Kyrölä, E., Tamminen, J., Sofieva, V., Fussen, D., Vanhellemont, F., Fanton d'Andon, O., Barrot, G., Blanot, L., Fehr, T., and Saavedra de Miguel, L.: Response of tropical stratospheric $O_3$, $NO_2$ and $NO_3$ to the equatorial Quasi-Biennial Oscillation and to temperature as seen from GOMOS/ENVISAT, Atmos. Chem. Phys. Discuss., 10, 9153–9171, doi:10.5194/acpd-10-9153-2010, 2010.

Hess, P.G. and Zbinden, R.: Stratospheric impact on tropospheric ozone variability and trends: 1990–200, Atmos. Chem. Phys., 13, 649–674, 2013.

Hofmann, D.J.: Recovery of Antarctic ozone hole, Nature 384, 222-223 doi:10.1038/384222a0, 1996.

Hood, L. L. and Soukharev, B. E.: Solar induced variations of odd nitrogen: Multiple regression analysis of UARS HALOE data, Geophys. Res. Lett., 33, L22805, doi:10.1029/2006GL028122, 2006.

Hurtmans, D., P. Coheur, C.Wespes, L. Clarisse, O. Scharf, C. Clerbaux, J. Hadji-Lazaro, M. George, and S. Turquety: FORLI radiative transfer and retrieval code for IASI, Journal of Quantitative Spectroscopy and Radiative Transfer, 113, 1391-1408, 2012.

Isaksen I. S. A., Zerefos, C. S., Kourtidis, K., Meleti, C., Dalsøren, S. B., Sundet, J. K., Grini, A., Zanis, P., and Balis, D.: Tropospheric ozone changes at unpolluted and semipolluted regions induced by stratospheric ozone changes, J. Geophys. Res., 110, D02302, doi:10.1029/2004JD004618, 2005.

Jiang, X., Pawson, S., Camp, C. D., Nielsen, E., Shia, R., Liao, T., Jeev, K., Limpasuvan, V., and Yung, Y. L.: Interannual variability and trends in extratropical ozone. Part II: Southern Hemisphere, J. Atmos. Sci., 65, 3030–3041, 2008.

Jones , A., J. Urban, D.P. Murtagh, P. Eriksson, S. Brohede, C. Haley, D. Degenstein, A. Bourassa, C. von Savigny, T. Sonkaew, A. Rozanov, H. Bovensmann, and J. Burrows, Evolution

of stratospheric ozone and water vapour time series studied with satellite measurements, *Atmos. Chem. Phys.*, *9* (16), 6055-6075, doi: 10.5194/acp-9-6055-2009, 2009.

Kuttippurath, J., F. Lefèvre, J.-P. Pommereau, H. K. Roscoe, F. Goutail, A. Pazmiño, and J. D. Shanklin: Antarctic ozone loss in 1979–2010: First sign of ozone recovery, Atmos. Chem. Phys.,1625–1635, 2013.

Kuttippurath, J., G. E. Bodeker, H. K. Roscoe, and P. J. Nair: A cautionary note on the use of EESC-based regression analysis for ozone trend studies, Geophys. Res. Lett.,42, 162–168, doi:10.1002/2014GL062142, 2015.

Kivi, R., Kyrö, E., Turunen, T., Harris, N. R. P., von der Gathen, P., Rex, M., Andersen, S. B., and Wohltmann, I.: Ozonesonde observations in the Arctic during 1989-2003: Ozone variability and trends in the lower stratosphere and free troposphere, J. Geophys. Res., 112, D08306, doi:10.1029/2006JD007271, 2007.

Knibbe J. S., R. J. van der A, and A. T. J. de Laat: Spatial regression analysis on 32 years of total column ozone data, Atmos. Chem. Phys., 14, 8461–8482, 2014.

Kramarova, N.A., E. R. Nash, P. A. Newman, P. K. Bhartia, R. D. McPeters, D. F. Rault, C. J. Seftor, P. Q. Xu, and G. J. Labow: Measuring the Antarctic ozone hole with the new Ozone Mapping and Profiler Suite (OMPS), Atmos. Chem. Phys., 14, 2353–2361, 2014.

Kyrölä, E., Tamminen, J., Leppelmeier, G. W., Sofieva, V., Hassinen, S., Seppälä, A., Verronen, P. T., Bertaux, J.-L., Hauchecorne, A., Dalaudier, F., Fussen, D., Vanhellemont, F., d'Andon, O. F., Barrot, G., Mangin, A., Theodore, B., Guirlet, M., Koopman, R., Saavedra, L., Snoeij, P., and Fehr, T.: Nighttime ozone profiles in the stratosphere and mesosphere by the Global Ozone Monitoring by Occultation of Stars on Envisat, J. Geophys. Res., 111, D24306, doi:10.1029/2006JD007193, 2006.

Kyrölä, E.; Tamminen, J.; Sofieva, V.; Bertaux, J. L.; Hauchecorne, A.; Dalaudier, F.; Fussen, D.; Vanhellemont, F.; Fanton d'Andon, O.; Barrot, G.; Guirlet, M.; Fehr, T. and Saavedra de Miguel, L.: GOMOS $O_3$, $NO_2$, and $NO_3$ observations in 2002–2008, Atmos. Chem. Phys., 10, 7723–7738, 2010, doi:10.5194/acp-10-7723-2010.

Kyrölä, E., Laine, M., Sofieva, V., Tukiainen, S., Tamminen, J., Päivärinta, S., Zawodny, J., and Thomason, L.: Combined SAGE II-GOMOS ozone profile data set for 1984–2011 and trend

952 analysis of the vertical distribution of ozone, Atmos. Chem. Phys., 13, 10645–10658,
953 doi:10.5194/acp-13-10645-2013, 2013.
954 Laine, M. , N. Latva-Pukkila, and E. Kyrölä: Analysing time-varying trends in stratospheric
955 ozone time series using the state space approach, Atmos. Chem. Phys., 14, 9707–9725, 2014.
956 Logan, J. A.: Tropospheric Ozone: Seasonal behaviour, Trends, and Anthropogenic Influence, J.
957 Geophys. Res., 90(D6), 10 463–10 482, 1985.
958 Logan, J. A., Jones, D. B. A., Megretskaia, I. A., Oltmans, S. J. Johnson, B. J., V¨omel, H.,
959 Randel, W. J., Kimani, W., and Schmidlin, F. J.: Quasi-biennial oscillation in tropical ozone as
960 revealed by ozonesonde and satellite data, J. Geophys. Res., 108(D8), 4244,
961 doi:10.1029/2002JD002170, 2003
962 Logan, J. A., Staehelin, J., Megretskaia, I. A., Cammas, J.-P. , Thouret, V., Claude, H., De
963 Backer, H., Steinbacher, M., Scheel, H.-E., Stübi, R.,, Fröhlich, M., and Derwent R.: Changes in
964 ozone over Europe: Analysis of ozone measurements from sondes, regular aircraft (MOZAIC)
965 and alpine surface sites, J. Geophys. Res., 117, D09301, doi:10.1029/2011JD016952, 2012.
966 Mäder, J. A., Staehelin, J., Brunner, D., Stahel, W. A., Wohltmann, I., and Peter, T.: Statistical
967 modelling of total ozone: Selection of appropriate explanatory variables, J. Geophys. Res., 112,
968 D11108, doi:10.1029/2006JD007694, 2007.
969 Mäder, J.A., J. Staehelin, T. Peter, D. Brunner, H. E. Rieder, and W. A. Stahel: Evidence for the
970 effectiveness of the Montreal Protocol to protect the ozone layer, Atmos. Chem. Phys., 10,
971 12161-12171, 2010.
972 Manney, G. L., Santee, M. L., Froidevaux, L., Hoppel, K., Livesey, N. J., and Waters, J. W.:
973 EOS MLS observations of ozone loss in the 2004-2005 Arctic winter, Geophys. Res. Lett., 33,
974 L04802, doi:10.1029/2005GL024494, 2006.
975 Manney, G. Santee, M. L., Rex, M., Livesey, N. J., Pitts, M.C., Veefkind, P., Nash, E. N.,
976 Wohltmann, I., Lehmann, R., Froidevaux, L., Poole, L. R., Schoeberl, M. R., Haffner, D.P.,
977 Davies, J., Dorokhov, V., Gernandt, H., Johnson, B., Kivi, R., Kyrö, E., Larsen, N., Levelt, P. F.,
978 Makshtas, A., McElroy, C. T., Nakajima, H., Parrondo, M.C., Tarasick, D. W., von der Gathen,
979 P., Walker, K. A., and Zinoviev, N. S. : Unprecedented Arctic ozone loss in 2011, Nature, 478,
980 469–475, doi:10.1038/nature10556, 2011.

McCormack, J.P., D.E. Siskind and L.L. Hood: Solar-QBO interaction and its impact on stratospheric ozone in a zonally averaged photochemical transport model of the middle atmosphere, J. Geophys. Res., 112, D16109, doi:10.1029/2006JD008369, 2007.

McLinden, C.A., S. Tegtmeier, and V. Fioletov, Technical note: A SAGE-corrected SBUV zonal-mean ozone data set, *Atmos. Chem. Phys.*, *9* (20), 7963-7972, doi: 10.5194/acp-9-7963-2009, 2009.

McPeters, R. D., Labow, G. J., and Logan, J. A.: Ozone climatological profiles for satellite retrieval algorithms, J. Geophys. Res.-Atmos., 112, D05308, doi:10.1029/2005JD006823, 2007.

Miller, A. J., Cai, A., Tiao, G., Wuebbles, D. J., Flynn, L. E., Yang, S.-K., Weatherhead, E. C., Fioletov, V., Petropavlovskikh, I., Meng, X.-L., Guillas, S., Nagatani, R. M., and Reinsel, G. C.: Examination of ozonesonde data for trends and trend changes incorporating solar and Arctic oscillation signals, J. Geophys. Res., 111, D13305, doi:10.1029/2005JD006684, 2006.

Nair, P. J., S. Godin-Beekmann, J. Kuttippurath, G. Ancellet, F. Goutail, A. Pazmiño, L. Froidevaux, J. M. Zawodny, R. D. Evans, H. J. Wang, J. Anderson, and M. Pastel: Ozone trends derived from the total column and vertical profiles at a northern mid-latitude station, Atmos. Chem. Phys., 13, 10373–10384, 2013.

Neu, J.L., T. Flury, G. L. Manney, M. L. Santee, N. J. Livesey and J. Worden, Tropospheric ozone variations governed by changes in stratospheric circulation, Nat. Geosc., 7, 340–344, doi:10.1038/ngeo2138, 2014.

Newchurch, M.J., Yang, E-S., Cunnold, D.M., Reinsel, G.C. and Zawodny, J.M.: Evidence for slowdown in stratospheric ozone loss: first stage of ozone recovery, J. Geophys. Res. Atmos., 108, D16, doi:10.1029/2003JD003471, 2003.

Oetjen, H., Payne, V.H., Kulawik, S.S., Eldering, A., Worden, J., Edwards, D.P., Francis, G.L., Worden, H.M., Clerbaux, C., Hadji-Lazaro, J., Hurtmans, D. : Extending the satellite data record of tropospheric ozone profiles from Aura-TES to MetOp-IASI, Atmos. Meas. Tech. Discuss., 7, 7013–7051, 2014.

Oltmans, S. J., Lefohn, A. S., Scheel, H. E., Harris, J. M., Levy II., H., Galbally, I. E., Brunke, E., Meyer, C. P., Lathrop, J. A., Johnson, B. J., Shadwick, D. S., Cuevas, E., Schmidlin, F. J., Tarasick, D.W., Claude, H., Kerr, J. B., Uchino, O., and Mohnen, V.: Trends of ozone in the troposphere, Geophys. Res. Lett., 25, 139–142, doi:10.1029/97GL03505, 1998.

1011 Oltmans, S. J., Lefohn, A. S., Harris, J. M., Galbally, I., Scheel, H. E., Bodeker, G., Brunke, E.,
1012 Claude, H., Tarasick, D., Johnson, B. J., Simmonds, P., Shadwick, D., Anlauf, K., Hayden, K.,
1013 Schmidlin, F., Fujimoto, T., Akagi, K., Meyer, C., Nichol, S., Davies, J., Redondas, A., and
1014 Cuevas, E.: Long-term changes in tropospheric ozone, Atmos. Environ., 40, 3156–3173, 2006.
1015 Parrington, M., P. I. Palmer, D. K. Henze, D. W. Tarasick, E. J. Hyer, R. C. Owen, D. Helmig,
1016 C. Clerbaux, K. W. Bowman, M. N. Deeter, E. M. Barratt, P.-F. Coheur, D. Hurtmans, Z. Jiang,
1017 M. George, and J. R. Worden: The influence of boreal biomass burning emissions on the
1018 distribution of tropospheric ozone over north America and the north Atlantic during 2010,
1019 Atmos. Chem. Phys., 12, 2077-2098, doi: 10.5194/acp-12-2077-2012, 2012.
1020 Parrish, D.D., K. S. Law, J. Staehelin, R. Derwent, O. R. Cooper,1, H. Tanimoto, A. Volz
1021 Thomas, S. Gilge,H.-E. Scheel, M. Steinbacher, and E. Chan: Long-term changes in lower
1022 tropospheric baseline ozone concentrations at northern mid-latitudes, Atmos. Chem. Phys., 12,
1023 11485–11504, 2012.
1024 Pitts, M. C., Poole, L. R., Dörnbrack, A., and Thomason, L. W.: The 2009–2010 Arctic polar
1025 stratospheric cloud season: a CALIPSO perspective, Atmos. Chem. Phys., 11, 2161–2177,
1026 doi:10.5194/acp-11-2161-2011, 2011.
1027 Pommier, M., C. Clerbaux, K. S. Law, G. Ancellet, P. Bernath, P.-F. Coheur, J. Hadji- Lazaro,
1028 D. Hurtmans, P. Nedelec, J.-D. Paris, F. Ravetta, T. B. Ryerson, H. Schlager, and A.
1029 J.Weinheimer: Analysis of IASI tropospheric $O_3$ data over the arctic during POLARCAT
1030 campaigns in 2008, Atmos. Chem. Phys., 12, 7371-7389, doi:doi:10.5194/acp-12-7371-2012,
1031 2012.
1032 Randel, W. J. and Wu, F.: Isolation of the ozone QBO in SAGE II data by singular-value
1033 decomposition, J. Atmos. Sci., 53, 2546– 2559, 1996.
1034 Randel, W. J. and Wu, F.: A stratospheric ozone profile data set for 1979-2005: Variability,
1035 trends, and comparisons with column ozone data, J. Geophys. Res.-Atmos., 112, D06313,
1036 doi:10.1029/ 2006JD007339, 2007.
1037 Reinsel, G. C., Weatherhead, E. C. , Tiao, G. C., Miller, A. J., Nagatani, R. M., Wuebbles, D. J.,
1038 and Flynn, L. E.: On detection of turnaround and recovery in trend for ozone, J. Geophys. Res.,
1039 107, D10, doi:10.1029/2001JD000500, 2002.

1040 Reinsel, G. C., Miller, A. J., Weatherhead, E. C., Flynn, L. E., Nagatani, R. M., Tiao, G. C., and
1041 Wuebbles, D. J.: Trend analysis of total ozone data for turnaround and dynamical contributions,
1042 J. Geophys. Res., 110, D16306, doi:10.1029/2004JD004662, 2005.
1043 Rodgers, C. D.: Inverse methods for atmospheric sounding: Theory and Practice, Series on
1044 Atmospheric, Oceanic and Planetary Physics, Vol. 2, World Scientific Publishing Co.,
1045 Singapore, 2000.
1046 Rieder, H. E., Frossard, L., Ribatet, M., Staehelin, J., Maeder, J. A., Di Rocco, S., Davison, A.
1047 C., Peter, T.,Weihs, P., and Holawe, F.: On the relationship between total ozone and atmospheric
1048 dynamics and chemistry at mid-latitudes – Part 2: The effects of the El Nino/Southern
1049 Oscillation, volcanic eruptions and contributions of atmospheric dynamics and chemistry to
1050 long-term total ozone changes, Atmos. Chem. Phys., 13, 165–179, doi:10.5194/acp-13- 165-
1051 2013, 2013.
1052 Safieddine S., Clerbaux C., George M., Hadji-Lazaro J., Hurtmans D., Coheur P.-F., Wespes C.,
1053 Loyola D., Valks P., Hao N.: Tropospheric ozone and nitrogen dioxide measurements in urban
1054 and rural regions as seen by IASI and GOME-2, J. Geophys. Res., 118, 18, 10555-10566, 2013.
1055 Salby, M., P. Callaghan, P. Keckhut, S. Godin, and M. Guirlet: Interannual changes of
1056 temperature and ozone: Relationship between the lower and upper stratosphere, J. Geophys.
1057 Res., 107(D18), 4342, doi:10.1029/2001JD000421, 2002.
1058 Salby, M., Titova, E., and Deschamps, L.: Rebound of Antarctic ozone, Geophys. Res. Lett., 38,
1059 L09702, doi:10.1029/2011GL047266, 2011.
1060 Santer, B.D., Wigley, T.M.L., Boyle, J.S., Gaffen, D.J., Hnilo, J.J., Nychka, D., Parker, D.E.,
1061 Parker, D.E. and Taylor, K.E.: Statistical significance of trends and trend differences in layer-
1062 average atmospheric temperature time series, J. Geophys. Res., 105(D6), 7337-7356, 2000.
1063 Saunois, M., Emmons, L., Lamarque, J.-F., Tilmes, S., Wespes, C., Thouret, V., and Schultz, M.:
1064 Impact of sampling frequency in the analysis of tropospheric ozone observations, Atmos. Chem.
1065 Phys., 12, 6757–6773, doi:10.5194/acp-12-6757-2012, 2012.
1066 Scannell, C., D. Hurtmans, A. Boynard, J. Hadji-Lazaro, M. George, A. Delcloo, A. Tuinder,
1067 P.F. Coheur, and C. Clerbaux: Antarctic ozone hole as observed by IASI/MetOp for 2008-2010,
1068 Atmos. Meas. Tech., 5, 123-139, 2012.

Schneider, M., Blumenstock, T., Hase, F., Höpfner, M., Cuevas, E., Redondas, A., and Sancho, J. M.: Ozone profiles and total column amounts derived at Izana Tenerife Island, from FTIR solar absorption spectra, and its validation by an intercomparison to ECC-sonde and Brewer spectrometer measurements, J. Quant. Spectros. Radiat. Transfer, 91, 3, 245–274, doi:10.1016/j.jqsrt.2004.05.067, 2005.

Shepherd, T.G., D. A. Plummer, J. F. Scinocca, M. I. Hegglin, V. E. Fioletov, M. C. Reader, E. Remsberg, T. von Clarmann, H. J. Wang: Reconciliation of halogen-induced ozone loss with the total-column ozone record, Nature Geoscience, 7, 443–449, doi:10.1038/ngeo2155, 2014.

Soukharev, B. E. and Hood, L. L.: Solar cycle variation of stratospheric ozone: Multiple regression analysis of long-term satellite data sets and comparisons with models, J. Geophys. Res.- Atmos., 111, D20314, doi:10.1029/2006JD007107, 2006.

Steinbrecht, W., Claude, H., and Winkler, P.: Enhanced upper stratospheric ozone: Sign of recovery or solar cycle effect?, J. Geophys. Res., 109, D02308, doi:10.1029/2003JD004284, 2004.

Steinbrecht, W., Claude, H., Schonenborn, F., McDermid, I. S., Leblanc, T., Godin, S., Song, T., Swart, D. P. J., Meijer, Y. J., Bodeker, G. E., Connor, B. J., Kampfer, N., Hocke, K., Calisesi, Y., Schneider, N., de la Noe, J., Parrish, A. D., Boyd, I. S., Brühl, C., Steil, B., Giorgetta, M. A., Manzini, E., Thomason, L. W., Zawodny, J. M., McCormick, M. P., Russell III, J. M., Bhartia, P. K., Stolarski, R. S., and Hollandsworth-Frith, S. M.: Long-term evolution of upper stratospheric ozone at selected stations of the Network for the Detection of Stratospheric Change (NDSC), J. Geophys. Res., 111, D10308, doi:10.1029/2005JD006454, 2006a.

Steinbrecht, W., Haßler, B., Br¨uhl, C., Dameris, M., Giorgetta, M. A., Grewe, V., Manzini, E., Matthes, S., Schnadt, C., Steil, B., and Winkler, P.: Interannual variation patterns of total ozone and lower stratospheric temperature in observations and model simulations, Atmos. Chem. Phys., 6, 349–374, doi:10.5194/acp-6-349-2006, 2006b.

Steinbrecht , W., H. Claude, F. Schönenborn, I.S. McDermid, T. Leblanc, S. Godin-Beekmann, P. Keckhut, A. Hauchecorne, J.A.E. Van Gijsel, D.P.J. Swart, G.E. Bodeker, A. Parrish, I.S. Boyd, N. Kämpfer, K. Hocke, R.S. Stolarski, S.M. Frith, L.W. Thomason, E.E. Remsberg, C. Von Savigny, A. Rozanov, and J.P. Burrows, Ozone and temperature trends in the upper

1098 stratosphere at five stations of the Network for the Detection of Atmospheric Composition
1099 Change, *Int. J. Remote Sens.*, *30*, 3875-3886, doi: 10.1080/01431160902821841, 2009.
1100 Stolarski, R. S. and Frith, S. M.: Search for evidence of trend slowdown in the long-term
1101 TOMS/SBUV total ozone data record: the importance of instrument drift uncertainty, Atmos.
1102 Chem. Phys., 6, 4057–4065, 2006.
1103 Tian, W., Chipperfield, M. P., Gray, L. J., and Zawodny, J. M.: Quasi-biennial oscillation and
1104 tracer distributions in a coupled chemistry-climate model, J. Geophys. Res., 111, D20301,
1105 doi:10.1029/2005JD006871, 2006.
1106 Varai, A., Homonnai, V., Jánosi, I.M., Müller, R. : Early signatures of ozone trend reversal over
1107 the Antarctic, Earth's Future, 3, 3, 95–109, doi:10.1002/2014EF000270, 2015.
1108 Vigouroux C., M. De Mazière, P. Demoulin, C. Servais, F. Hase, T. Blumenstock, I. Kramer, M.
1109 Schneider, J. Mellqvist, A. Strandberg, V. Velazco, J. Notholt, R. Sussmann, W. Stremme, A.
1110 Rockmann, T. Gardiner, M. Coleman, and P. Woods, Evaluation of tropospheric and
1111 stratospheric ozone trends over Western Europe from ground-based FTIR network observations,
1112 Atmos. Chem. Phys., 8 (23), 6865-6886, doi: 10.5194/acp-8-6865-2008, 2008.
1113 Vigouroux, C., T. Blumenstock, M. Coffey, Q. Errera, O. García, N. B. Jones, J. W. Hannigan,
1114 F. Hase, B. Liley, E. Mahieu, J. Mellqvist, J. Notholt, M. Palm, G. Persson, M. Schneider, C.
1115 Servais, D. Smale, L. Thölix, and M. De Mazière: Trends of ozone total columns and vertical
1116 distribution from FTIR observations at 8 NDACC stations around the globe, Atmos. Chem.
1117 Phys. Discuss., 14, 24623–24666, 2014.
1118 Weatherhead, E. C. and Andersen, S. B.: The search for signs of recovery of the ozone layer,
1119 Nature, 441, 39–45, doi:10.1038/nature04746, 2006.
1120 Weiss, A.K., J. Staehelin, C. Appenzeller, and N.R.P. Harris, Chemical and dynamical
1121 contributions to ozone profile trends of the Payerne (Switzerland) balloon soundings, *J.*
1122 *Geophys. Res.*, 106 (D19), 22685-22694, 2001.
1123 Wespes, C., Hurtmans, D., Clerbaux, C., Santee, M. L., Martin, R. V., and Coheur, P. F.: Global
1124 distributions of nitric acid from IASI/MetOP measurements, Atmos. Chem. Phys., 9, 7949–7962,
1125 doi:10.5194/acp-9-7949-2009, 2009.
1126 Wespes, C., L. Emmons, D. P. Edwards, J. Hannigan, D. Hurtmans, M. Saunois, P.-F. Coheur,
1127 C. Clerbaux, M. T. Coffey, R. L. Batchelor, R. Lindenmaier, K. Strong, A. J. Weinheimer, J. B.

Nowak, T. B. Ryerson, J. D. Crounse, and P. O. Wennberg: Analysis of ozone and nitric acid in spring and summer arctic pollution using aircraft, ground-based, satellite observations and mozart-4 model: source attribution and partitioning, Atmos. Chem. Phys., 12, 237-259, 2012.

Wilson, R. C., Fleming, Z. L., Monks, P. S., Clain, G., Henne, S., Konovalov, I. B., Szopa, S., and Menut, L.: Have primary emission reduction measures reduced ozone across Europe? An analysis of European rural background ozone trends 1996–2005, Atmos. Chem. Phys., 12, 437–454, doi:10.5194/acp-12-437-2012, 2012.

WMO: Scientific Assessment of Ozone Depletion: 2002, Global Ozone Research and Monitoring Project –Report No. 47, World Meteorological Organization, Geneva, Switzerland, 2003.

WMO: Scientific Assessment of Ozone Depletion: 2006, Global Ozone Research and Monitoring Project– Report 50, World Meteorological Organization, Geneva, Switzerland, 2007.

WMO: Scientific Assessment of Ozone Depletion: 2010, Global Ozone Research and Monitoring Project–Report 52, World Meteorological Organization), Geneva, Switzerland, 2011.

WMO : Scientific Assessment of Ozone Depletion: 2014, Global Ozone Research and Monitoring Project– Report 56, World Meteorological Organization, Geneva, Switzerland, 2014.

Yang, E.-S., Cunnold, D. M., Salawitch, R. J., McCormick, M. P., Russell, J., Zawodny, J. M., Oltmans, S., and Newchurch, M. J.: Attribution of recovery in lower-stratospheric ozone, J. Geophys. Res., 111, D17309, doi:10.1029/2005JD006371, 2006.

**Table 1** List of the proxies used in this study and their sources

| Proxy | Description (*resolution*) | Sources |
|---|---|---|
| **F10.7** | The 10.7 cm solar radio flux (*daily or monthly*) | NOAA National Weather Service Climate Prediction Center: ftp://ftp.ngdc.noaa.gov/STP/space-weather/solar-data/solar-features/solar-radio/noontime-flux/penticton/penticton_adjusted/listings/listing_drao_noontime-flux-adjusted_daily.txt or ftp://ftp.ngdc.noaa.gov/STP/space-weather/solar-data/solar-features/solar-radio/noontime-flux/penticton/penticton_adjusted/listings/listing_drao_noontime-flux-adjusted_monthly.txt |
| **$QBO^{10}$** **$QBO^{30}$** | Quasi-Biennial Oscillation index at 10hPa and 30hPa (*monthly*) | Free University of Berlin: www.geo.fu-berlin.de/en/met/ag/strat/produkte/qbo/ |
| **ENSO** | El Niño /Southern Oscillation - Nino 3.4 Index (*3-monthly averages*) | NOAA National Weather Service Climate Prediction Center: http://www.cpc.noaa.gov/data/indices/ |
| **NAO** | North Atlantic Oscillation index (*daily or monthly*) | ftp://ftp.cpc.ncep.noaa.gov/cwlinks/norm.daily.nao.index.b500101.current.ascii or http://www.cpc.ncep.noaa.gov/products/precip/CWlink/pna/norm.nao.monthly.b5001.current.ascii |
| **AAO** | Antarctic Oscillation index (*daily or monthly*) | ftp://ftp.cpc.ncep.noaa.gov/cwlinks/norm.daily.aao.index.b790101.current.ascii or http://www.cpc.ncep.noaa.gov/products/precip/CWlink/daily_ao_index/aao/monthly.aao.index.b79.current.ascii |

**Table 2** Ozone trends and associated uncertainties (95% confidence limits; accounting for the autocorrelation in the noise residuals), given in DU/year, for 20-degree latitude bands, based on daily (top values) and monthly (bottom values) medians over 6 years of IASI observations. Bold (underlined) values refer to significant (positive) trends. Values marked with a star (*) refer to trends which are rejected by the iterative backward elimination procedure†.

| ***DU/ yr*** | **# Days** | **Ground-300hPa (MLT)** | **300-150hPa (UTLS)** | **150-25hPa (MLST)** | **25-3hPa (UST)** | **Total columns** |
|---|---|---|---|---|---|---|
| **70°N-90°N (Feb-Oct)** | 1493 | **-0.13±0.10**<br>-0.03±0.29* | **1.28±0.82**<br>0.70±0.92* | **2.81±2.27**<br>-0.04±2.60* | -0.16±0.97*<br>-1.81±2.81* | **3.90±2.93**<br>1.37±3.62* |
| **50°N-70°N** | 2103 | -0.08±0.09<br>0.17±0.35* | **0.73±0.51**<br>1.24±1.24 | 0.97±1.30<br>2.28±4.24* | **0.55±0.36**<br>0.66±0.76 | **1.93±1.71**<br>4.72±5.58 |
| **30°N-50°N** | 2105 | **-0.19±0.05**<br>**-0.15±0.13** | **0.34±0.18**<br>0.75±0.75 | -0.34±0.77<br>-0.37±1.65* | **0.89±0.41**<br>**0.87±0.52** | 0.91±1.24<br>0.33±2.25* |
| **10°N-30°N** | 2105 | 0.10±0.11<br>0.12±0.15* | -0.03±0.10*<br>0.05±0.12* | **-0.73±0.29**<br>-0.55±0.62* | **0.95±0.65**<br>**1.25±0.74** | 0.21±0.30*<br>0.82±1.01 |
| **10°S-10°N** | 2104 | **-0.41±0.12**<br>**-0.25±0.14** | **-0.25±0.07**<br>-0.08±0.10 | -0.11±0.26*<br>-0.11±0.64* | **0.44±0.19**<br>0.61±0.64 | -0.16±0.34<br>0.13±0.83* |
| **30°S-10°S** | 2106 | **-0.22±0.10**<br>**-0.15±0.13** | **-0.08±0.04**<br>**-0.09±0.07** | **-0.61±0.26**<br>**-0.45±0.36** | **0.89±0.58**<br>0.80±1.23 | -0.04±0.31*<br>-0.01±1.26* |
| **50°S-30°S** | 2105 | **-0.19±0.07**<br>**-0.18±0.09** | **-0.22±0.08**<br>**-0.27±0.12** | **-2.17±0.58**<br>**-2.36±1.80** | **1.74±0.77**<br>1.21±1.30 | -0.79±0.96<br>-0.64±1.45* |
| **70°S-50°S** | 2105 | **-0.13±0.05**<br>*-0.22±0.12* | 0.09±0.16<br>0.05±0.32* | 0.56±0.82<br>0.02±1.15* | **0.54±0.29**<br>0.57±0.82 | 1.15±1.28<br>0.51±1.75* |
| **90°S-70°S (Oct-Apr)** | 738 | -0.15±0.21*<br>-0.17±0.40* | 0.01±0.61*<br>0.25±0.73* | 0.00±2.36*<br>2.59±3.80* | **1.04±0.57**<br>0.91±2.10* | 1.50±3.15*<br>3.28±5.12* |

† The trend values result from the adjustment of the regression model where the linear term is kept whatever its p-value calculated during the iterative process.

**Table 3** Same as Table 2 but for seasonal $O_3$ trends and associated uncertainties based on daily medians during JJA (top values) and DJF (bottom values) periods. Values marked with a star (*) refer to trends which are rejected by the iterative backward elimination procedure†.

| *DU/ yr* | # Days | Ground-300hPa (MLT) | 300-150hPa (UTLS) | 150-25hPa (MLST) | 25-3hPa (UST) | Total columns |
|---|---|---|---|---|---|---|
| **70°N-90°N** | 613 | **-0.18±0.08** | **1.13±0.65** | -0.91±1.52 | **1.72±0.51** | **1.36±1.15** |
| **(Feb-Oct)** | 48 | - | - | - | - | - |
| **50°N-70°N** | 551 | **-0.23±0.07** | **1.03±0.37** | 0.62±1.64 | **1.67±0.48** | **3.01±1.64** |
| | 527 | -0.09±0.12* | **1.74±1.30** | 0.73±1.73* | -0.66.±0.79 | 1.56±2.66* |
| **30°N-50°N** | 551 | **-0.30±0.10** | **0.42±0.30** | -0.30±0.65* | **0.84±0.25** | 1.17±1.35 |
| | 529 | **-0.24±0.09** | 0.28±0.28 | -0.82.±0.90 | **0.62.±0.49** | -0.81.±1.05 |
| **10°N-30°N** | 551 | -0.05±0.16* | **0.17±0.05** | **-0.34±0.30** | **0.36±0.27** | -0.09±0.54* |
| | 529 | **0.18±0.14** | 0.01.±0.09* | **-1.05.±0.45** | 0.49±0.54* | -1.14±0.44 |
| **10°S-10°N** | 551 | -0.06.±0.10 | 0.04±0.05* | -0.84±0.86 | 0.32±0.42 | -0.56±0.74 |
| | 529 | **-0.70.±0.23** | **-0.32±0.10** | 1.64±1.77 | 0.53±0.59 | 0.34±0.93* |
| **30°S-10°S** | 551 | **-0.26±0.09** | -0.06±0.07 | **-0.56±0.40** | **1.06±0.55** | 0.24±0.43 |
| | 530 | **-0.15±0.11** | 0.06±0.12* | -0.12±0.31* | **1.48±0.53** | **1.56±0.92** |
| **50°S-30°S** | 551 | **-0.21±0.05** | **-0.16±0.09** | -0.52±0.54 | 0.49±0.59 | -0.44±0.83 |
| | 529 | **-0.10±0.06** | **-0.14±0.06** | **-2.83±0.64** | **3.40±0.85** | 0.47±0.52 |
| **70°S-50°S** | 551 | **-0.25±0.06** | **1.03±0.60** | **2.63±1.65** | **0.98±0.62** | **3.44±2.47** |
| | 529 | **-0.10±0.04** | 0.19±0.24* | **0.52±0.48** | **1.66±0.70** | **1.72±0.74** |
| **90°S-70°S** | - | - | - | - | - | - |
| **(Oct-Apr)** | 523 | **-0.21±0.20** | -0.46±0.80* | 0.16±2.53* | **1.18±0.67** | 0.98±3.27* |

† The trend values result from the adjustment of the regression model where the linear term is kept whatever its p-value calculated during the iterative process.

**Table 4** Ozone trends and associated uncertainties (95% confidence limits), given in DU/year over NDACC (Network for the Detection of Atmospheric Composition Change) stations in the N.H. based on daily medians of IASI (within a grid box of 1°x1° centered on stations, two first rows) and FTIR observations (successive rows for different time intervals). Italic values (2$^{d}$ row) refer to trends inferred from subsampled IASI data and bold values refer to statistically significant trends. Values marked with a star (*) refer to trends which are rejected by the iterative backward elimination procedure$^{\dagger}$.

| ***DU/yr*** | **Data periods** | **# days** | **25-3hPa (US)** | **Total columns** |
|---|---|---|---|---|
| Ny-Alesund (79°N) Mar-Sept | 2008-2013 | 1239 | 0.56±0.73 | **5.26±4.72** |
| | *Subsamp. 2008-2012* | *82* | *-0.29±4.58* | *6.26±18.11* |
| | 2008-2012 | 84 | -3.58±4.58 | 2.24±20.78* |
| | 2003-2012 | 168 | -0.17±0.70* | **-4.84±3.01** |
| | 2000-2012 | 288 | **0.64±0.60** | -1.02±2.40* |
| | 1999-2012 | 320 | **0.62±0.55** | **-2.35±1.40** |
| | 1995-2012 | 383 | **1.03±0.66** | 1.31±2.39* |
| | 1995-2003 | 167 | **1.25±1.05** | 3.33±3.41 |
| Thule (77°N) Mar-Sept | 2008-2013 | 1094 | **1.24±1.09** | **4.97±4.72** |
| | *Subsamp. 2008-2012* | *231* | *1.31±2.69* | *0.10±7.36* |
| | 2008-2012 | 340 | -2.10±2.89 | 0.39±11.59* |
| | 2003-2012 | 697 | 0.86±0.89 | -2.77±2.99 |
| | 2000-2012 | 776 | **1.33±0.86** | -1.29±1.73 |
| | 1999-2012 | 779 | **1.69±0.88** | -1.25±1.74 |
| | 1999-2003 | 138 | **3.73±2.90** | 4.86±10.13* |
| Kiruna (68°N) Mar-Sept | 2008-2013 | 1236 | 0.21±1.42 | **4.41±4.00** |
| | *Subsamp. 2008-2012* | *226* | *0.97±4.05* | *3.78±6.03* |
| | 2008-2012 | 254 | -1.97±6.04* | -3.75±6.64* |
| | 2003-2012 | 678 | 0.15±0.67* | 2.26±3.68 |
| | 2000-2012 | 913 | **1.60±1.29** | 3.69±4.20 |
| | 1999-2012 | 984 | **1.10±0.98** | -0.43±1.64* |
| | 1996-2012 | 1183 | **1.11±0.54** | **1.82±1.77** |
| | 1996-2003 | 596 | **1.26±1.21** | 1.12±3.77* |
| Jungfraujoch (47°N) | 2008-2013 | 1580 | **2.95±0.61** | **5.64±3.15** |
| | *Subsamp. 2008-2012* | *524* | ***3.72±1.14*** | ***5.61±5.11*** |
| | 2008-2012 | 565 | 1.60±1.80 | **5.28±4.82** |
| | 1998-2012 | 1582 | 0.10±0.35 | -0.28±0.86* |
| | 1995-2012 | 1771 | 0.02±0.33* | **0.85±0.79** |

| | | | | |
|---|---|---|---|---|
| Zugspitze (47°N) | 2008-2013 | 1729 | **3.17±0.56** | **5.53±2.92** |
| | *Subsamp.* | | | |
| | *2008-2012* | *538* | ***3.56±1.63*** | ***5.99±4.49*** |
| | 2008-2012 | 597 | 0.71±1.22 | 3.46±3.79 |
| | 1998-2012 | 1472 | 0.08±0.32* | 0.81±0.98 |
| | 1995-2012 | 1525 | 0.23±0.32 | **1.36±1.01** |
| Izana (28°N) | 2008-2013 | 1803 | 0.56±0.65 | **1.28±0.77** |
| | *Subsamp.* | | | |
| | *2008-2012* | *380* | *0.32±1.28* | *0.11±1.95* |
| | 2008-2012 | 443 | 0.24±0.80* | 0.91±2.44* |
| | 1999-2012 | 1257 | **0.46±0.25** | 0.20±0.33* |

† The trend values result from the adjustment of the regression model where the linear term is kept whatever its p-value calculated during the iterative process.

## Figure captions

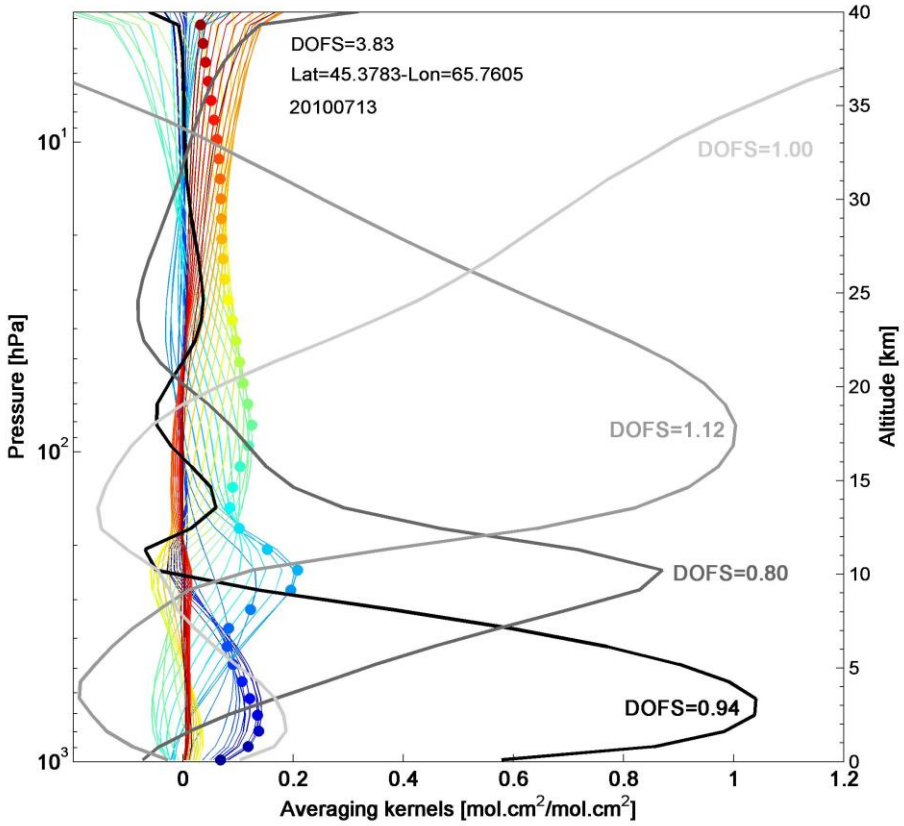


**Figure 1.** Typical IASI FORLI-$O_3$ averaging kernels, in partial column units, corresponding to one mid-latitude observation in July (45°N/66°E) for each 1 km retrieved layers from ground to 40 km altitude (color scale) and for 4 merged layers: ground-300 hPa; 300-150 hPa; 150-25 hPa; 25-3 hPa (grey lines). The total DOFS and the DOFS for each merged layers are also indicated.

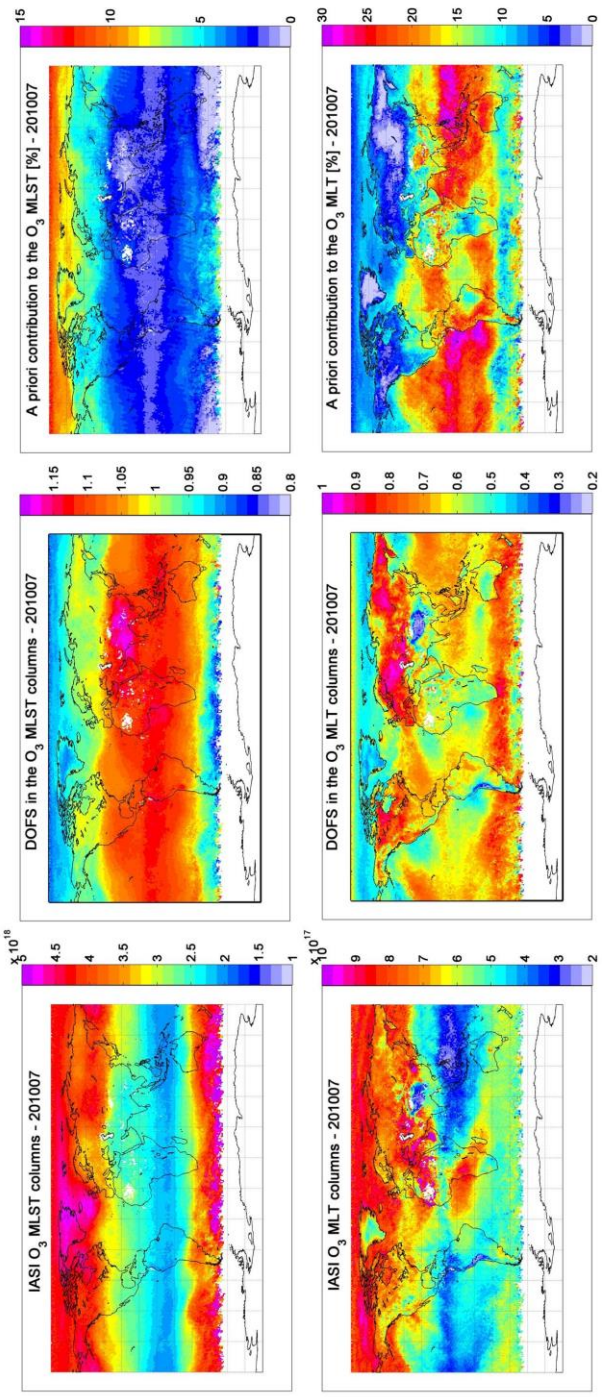


1238

1239 **Figure 2.** Distributions of (a) $O_3$ columns, (b) DOFS and (c) *a priori* contribution (given as a %)
1240 in the ground-300hPa (MLT) and 150-25hPa (MLST) layers for IASI $O_3$, averaged over July
1241 2010 daytime data. Note that the scales are different.

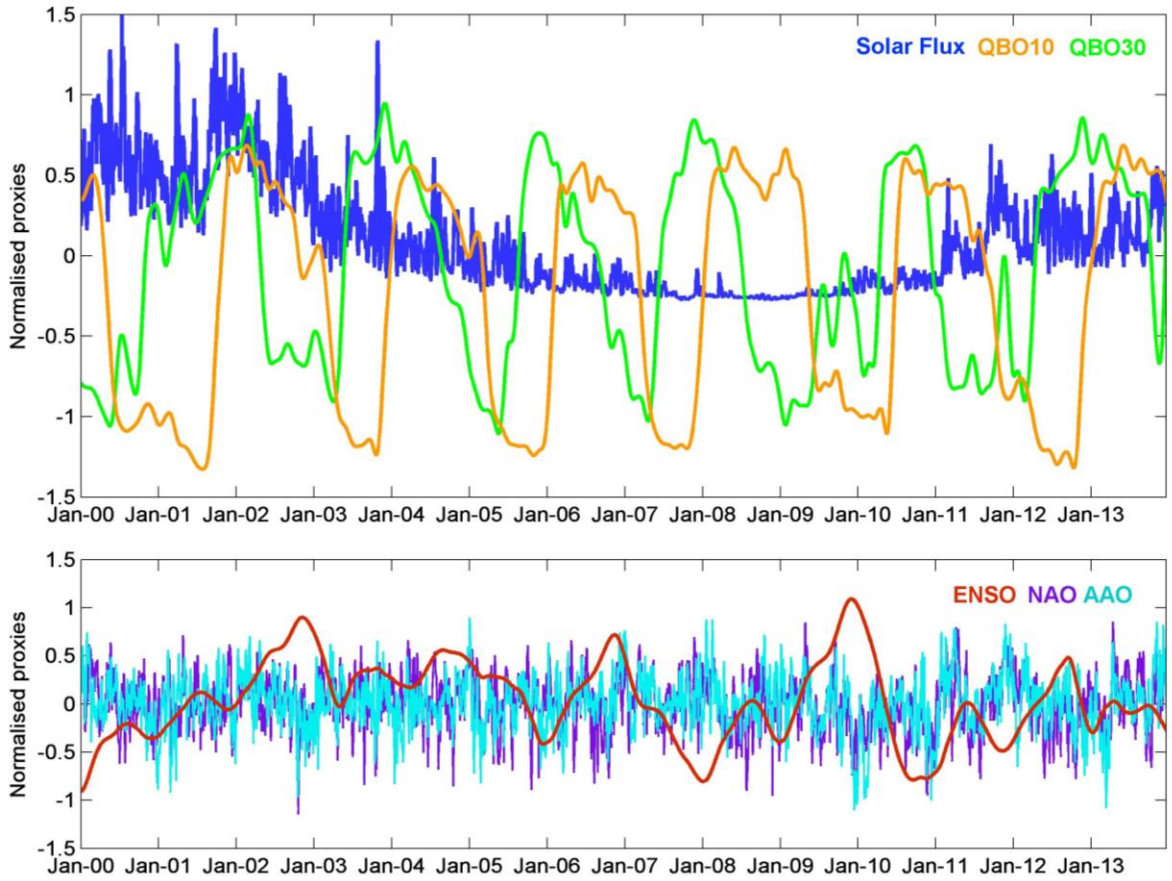


**Figure 3.** Normalized proxies as a function of time for the period 2000-2013 for the solar F10.7 cm radio flux (blue) and the equatorial winds at 10 (green) and 30 hPa (orange), respectively (top panel), and for the El Niño (red), north Atlantic oscillation (purple) and Antarctic oscillation (light blue) indexes (bottom panel).

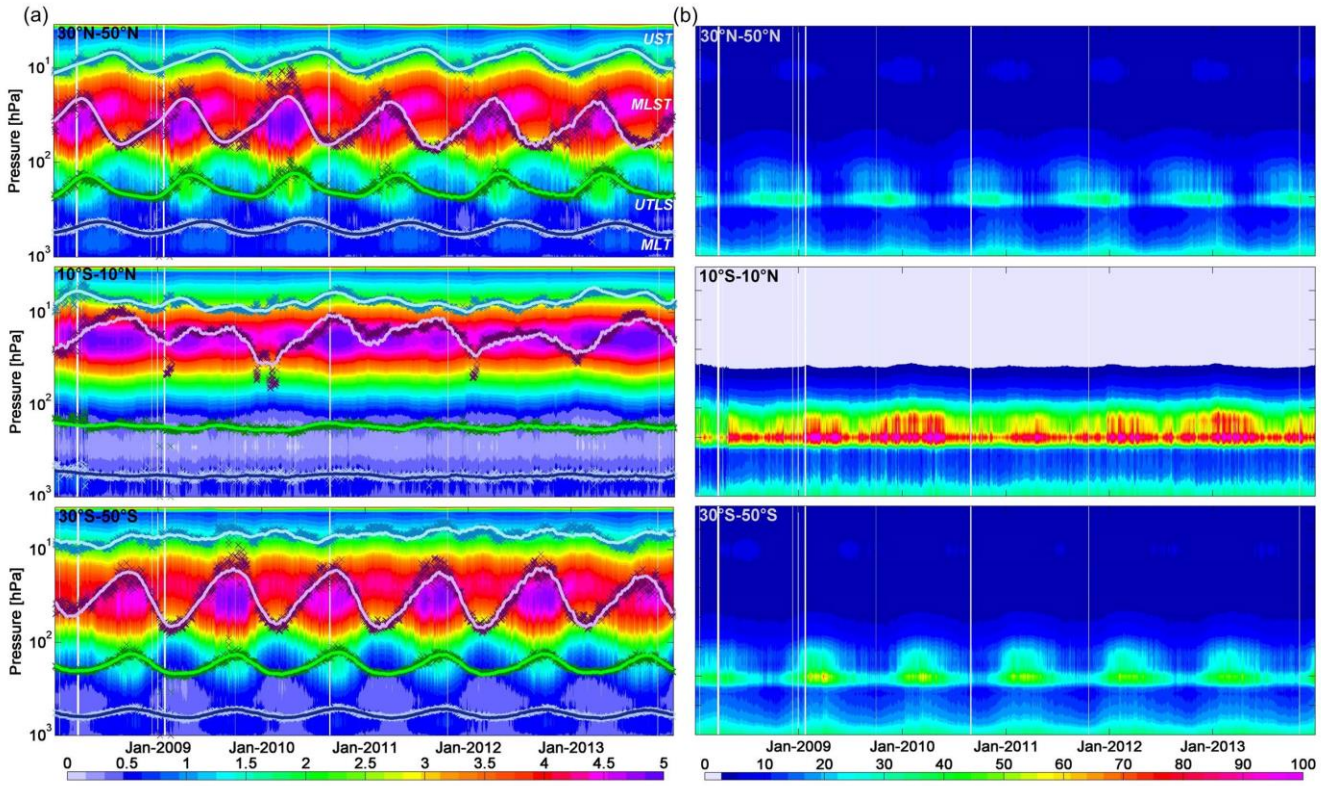


**Figure 4.** (a) Daily IASI $O_3$ profiles ($1x10^{12}$ molecules/$cm^3$) for the period 2008-2013 and over the range of the retrieved profiles as a function of time and altitude, in three latitude bands: 30°N-50°N (top), 10°S-10°N (middle), 30°S-50°S (bottom). Superimposed daily IASI $O_3$ partial columns (scatters) and the associated fits (solid lines) from the multivariate regressions for the MLT (ground-300hPa), UTLS (300-150hPa), MLST (150-25hPa) and UST (above 25hPa) layers. The IASI measurements and the fits have been scaled for clarity. (b) Estimated total retrieval errors (%) associated with daily IASI $O_3$ profiles.

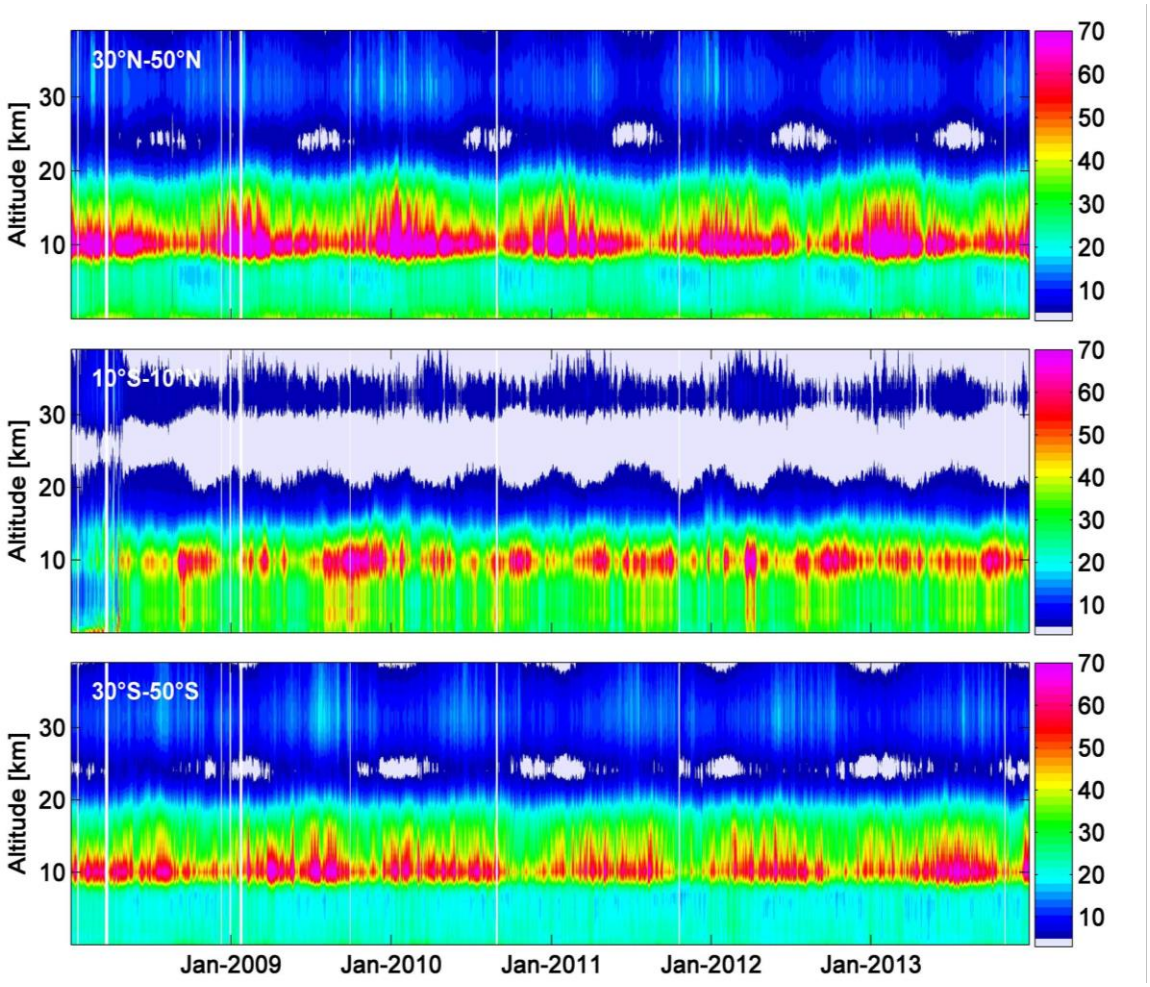


**Figure 5.** Daily IASI $O_3$ variability (%), expressed as $[\sigma(O_3(t))/O_3(t)]\times 100\%$, where σ is the standard deviation, as a function of time and altitude in three latitude bands: 30°N-50°N (top), 10°S-10°N (middle), 30°S-50°S (bottom).

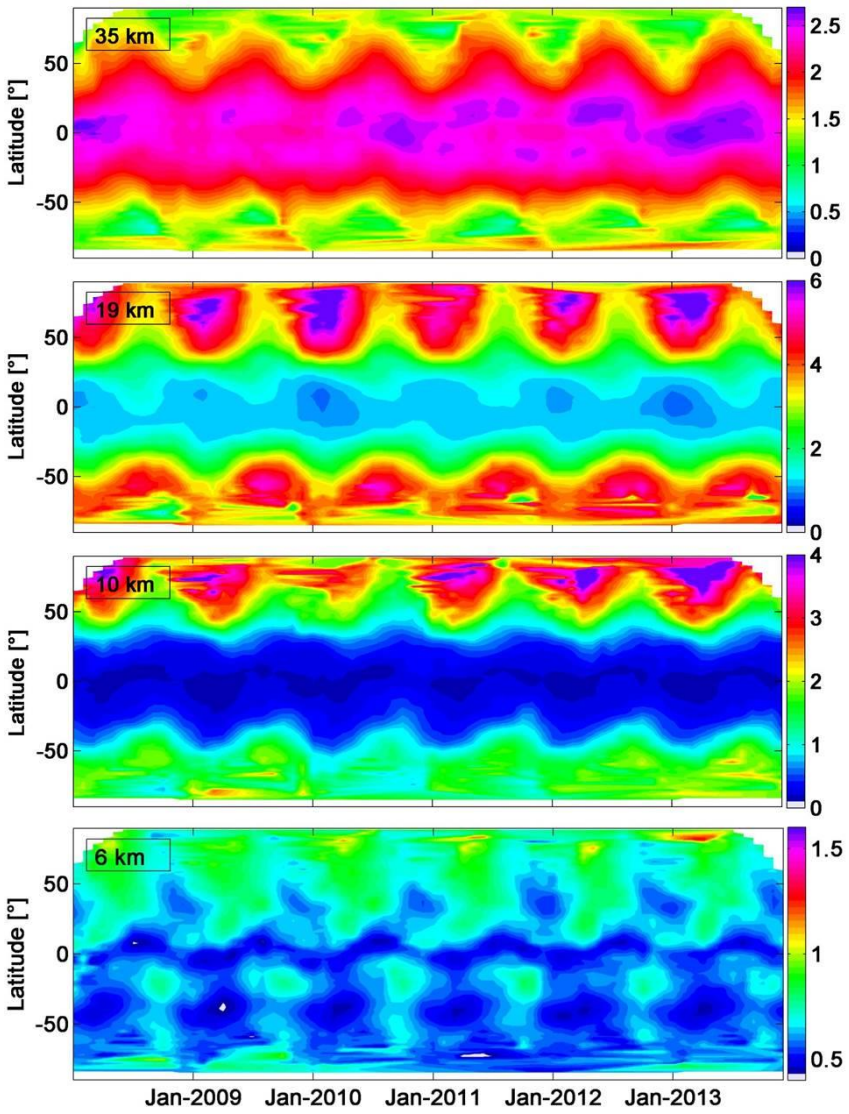


1271

1272 **Figure 6.** Daily IASI $O_3$ number density ($1x10^{12}$ molecules/$cm^3$) at 35 km (top row), 19 km
1273 (second row), 10 km (third row) and 6 km (bottom row) as a function of time and latitude. Note
1274 that the color scales are different.

1275

1276

1277

1278

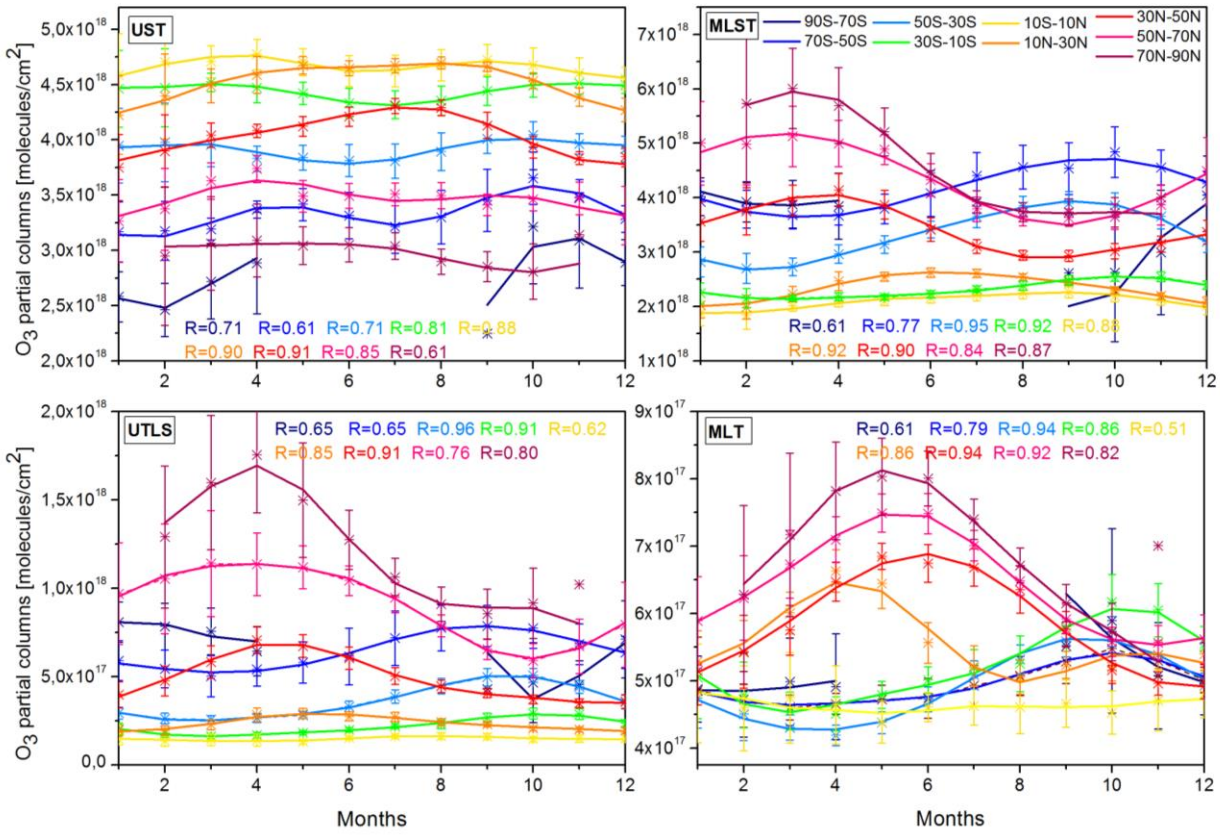


**Figure 7.** Monthly medians of measured (scatters) and of fitted (line) IASI $O_3$ columns averaged over the period 2008-2013, for the UST, MLST, UTLS and MLT layers and for each 20-degrees latitude bands (color scale in the top-right panel). The fit is based on daily medians. Error bars give the 1σ standard deviation relative to the monthly median values. Correlation coefficient (R) between the daily median observations and the fit are also indicated. Note that the scales are different.

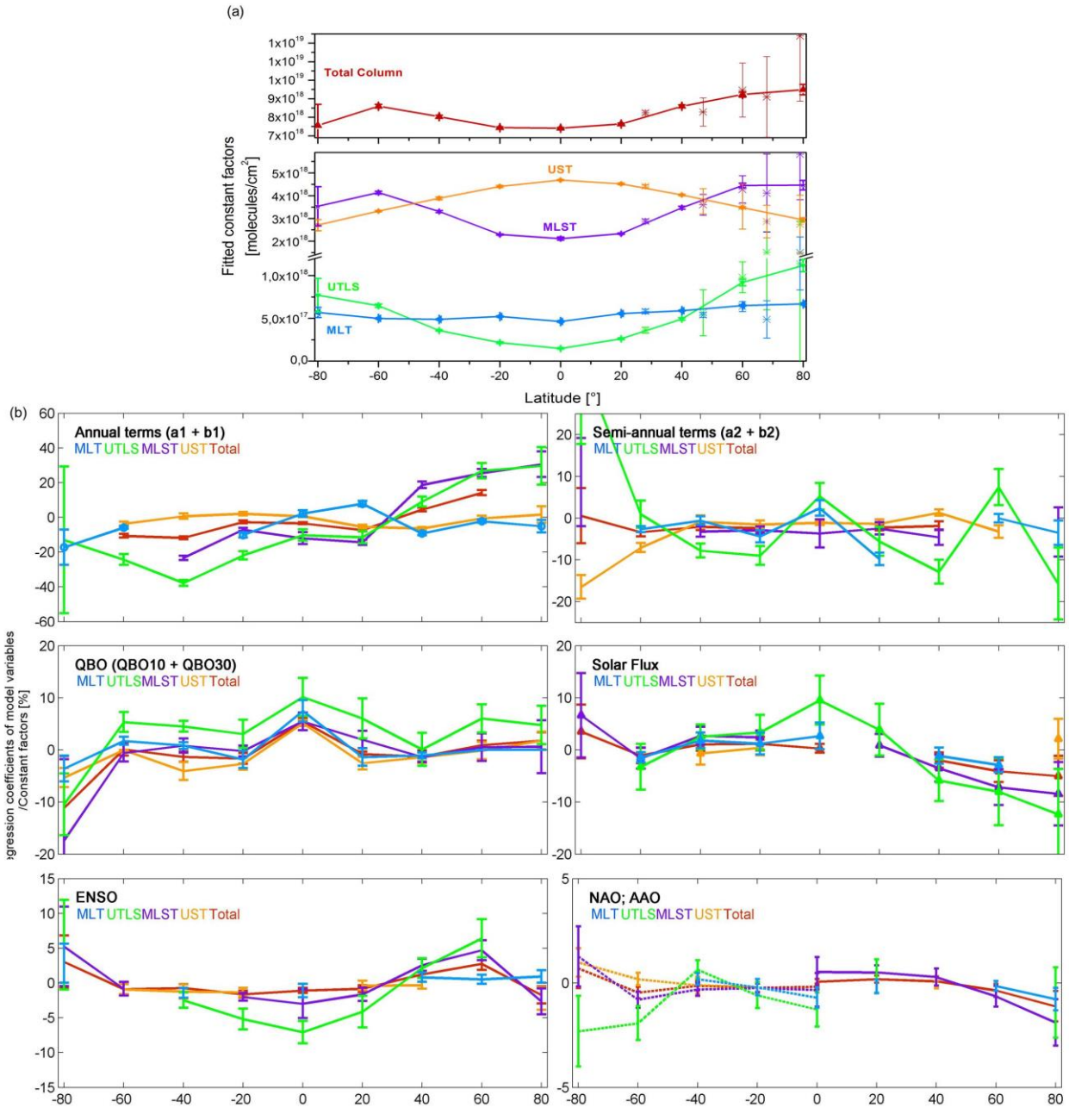


**Figure 8.** (a) Fitted constant factors (Cst, see Eq.1, Section 3) from the 6-years IASI daily $O_3$ time series for the 20-degree latitude belts, separately given for the 4 layers and for the total column. The stars correspond to the constant factors fitted above ground-based measurement stations: Ny-Ålesund (79°N), Kiruna (68°N), Harestua (60°N), Jungfraujoch (47°N), Izana (28°N). (b) Regression coefficients of the variables retained by the stepwise procedure, given in % as $\left[regression\_coefficient / fitted\_cst\right] \times 100\%$. Identification for the variables: Annual (top

left) and Semi-Annual variations (top right) terms, QBO at 10 and 30 hPa (bottom left), solar flux (bottom right). Note that the scales are different. The associated fitting uncertainties (95% confidence limits) are also represented (error bars).

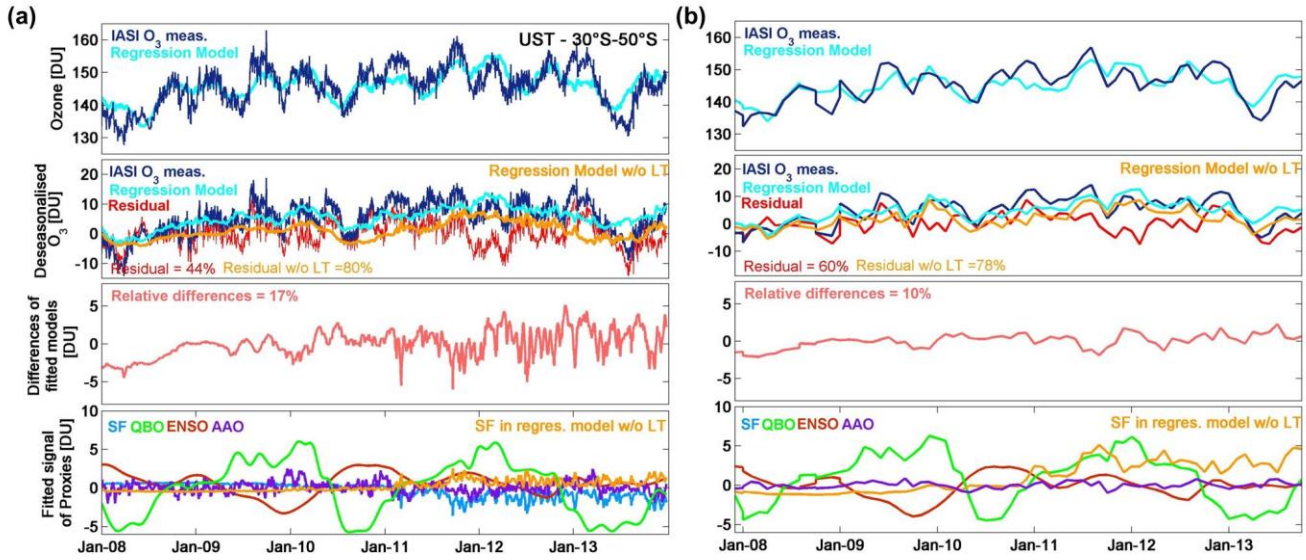


**Figure 9.** Daily (a) and monthly (b) time series of $O_3$ measurements and of the fitted regression model in the UST for the 30°S-50°S latitude band (top row), of the deseasonalised $O_3$ ($2^d$ row), of the difference of the fitted models with and without the linear term ($3^d$ row), and of the fitted signal of proxies $\left[regression\_coefficient \times proxy\right]$: SF (blue), QBO ($QBO^{10}$ + $QBO^{30}$; green), ENSO (red) and AAO (purple) (bottom) (given in DU). The averaged residuals relative to the deseasonalised IASI time series are also indicated (%).

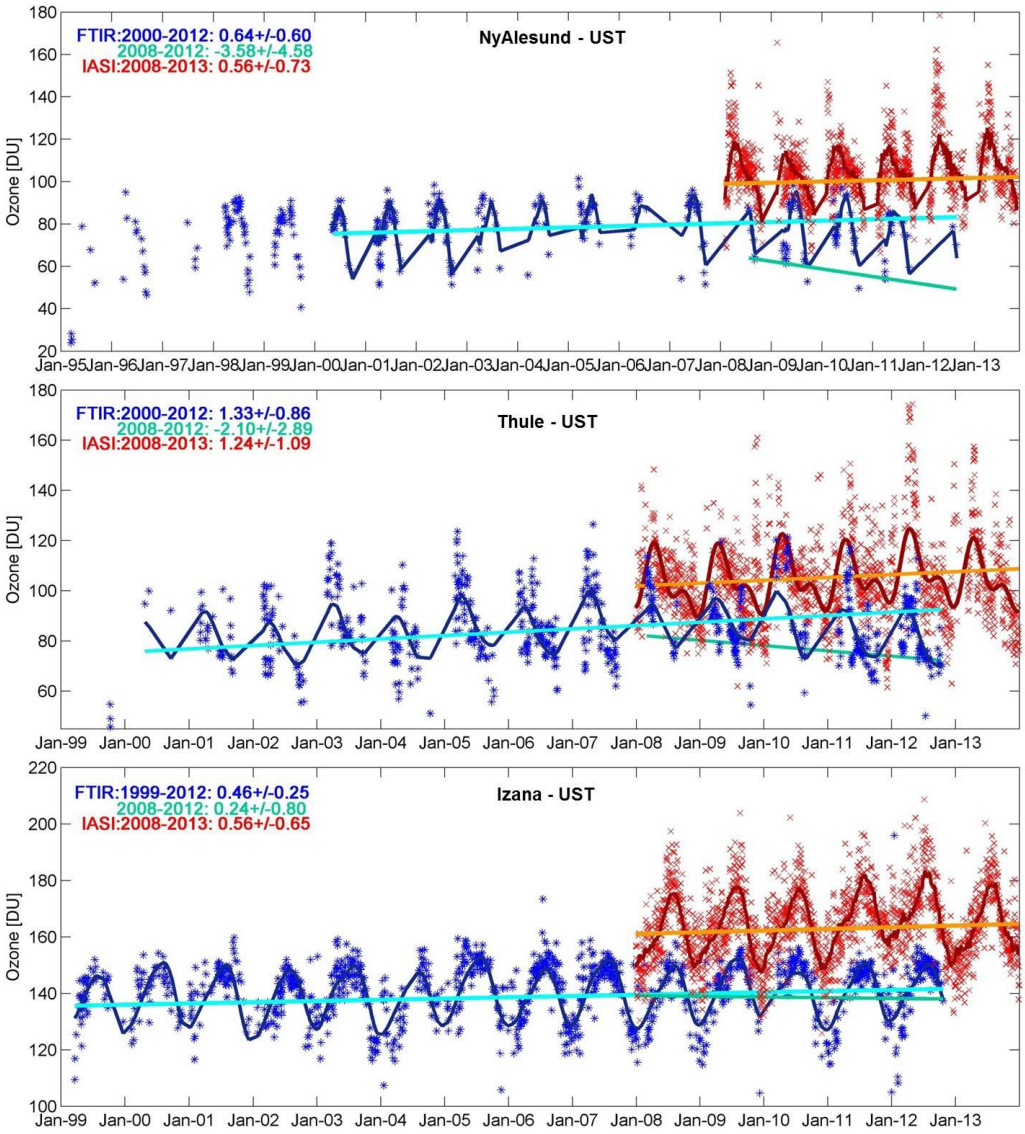


**Figure 10.** Daily time series of $O_3$ FTIR (blue symbols) and IASI (red symbols) measurements in the UST at Ny-Alesund (top), Thule (middle) and Izana (bottom), covering the 1995-2012 and the 1999-2012 periods, respectively (given in DU). The fitted regression models (dark blue and dark red lines, for FTIR and IASI, respectively) and the linear trends calculated for periods starting after the turnaround over 1999/2000-2012 and over 2008-2012 for FTIR (light blue and green lines), and the 2008-2013 period for IASI (orange line) are also represented (DU/yr). The trend values given in DU/year are indicated.